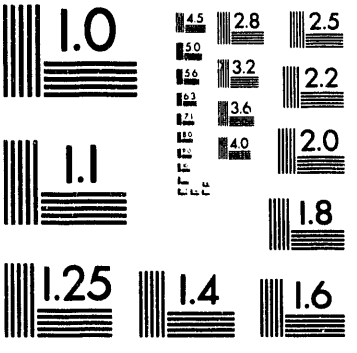
1.0
1.1
1.25
1.4
1.6
1.8
2.0
2.2
2.5
2.8
3.2
3.6
4.0
4.5
5.0
5.6
6.3
7.1
8.0
9.0

1 of 1

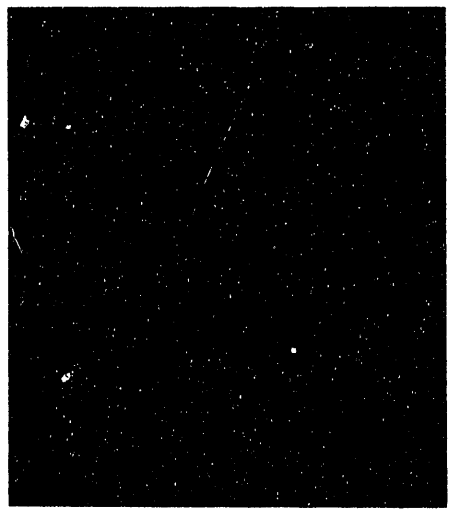

Energy Conversion & Storage Program 1992 Annual Report

Elton J. Cairns, Program Leader

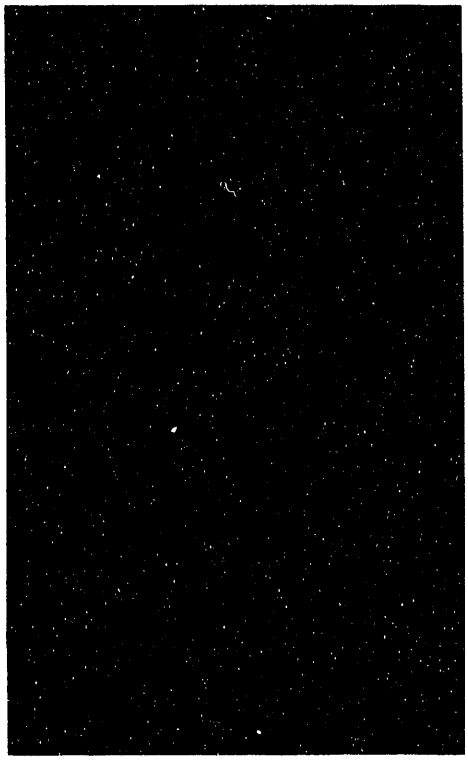

Energy & Environment Division
Lawrence Berkeley Laboratory
University of California
Berkeley, California 94720
(510) 486-5001

Report No. LBL 33444

Contents

Introduction

The Energy Conversion and Storage Program applies principles of chemistry and materials science to solve problems in several areas: 1) production of new synthetic fuels, 2) development of high-performance rechargeable batteries and fuel cells, 3) development of advanced thermochemical processes for energy conversion, 4) characterization of complex chemical processes and chemical species, and 5) study and application of novel materials for energy conversion and transmission. Projects focus on transport-process principles, chemical kinetics, thermodynamics, separation processes, organic and physical chemistry, novel materials, and advanced methods of analysis.

Electrochemistry research aims to develop advanced power systems for electric vehicle and stationary energy storage applications. Topics include the identification of new electrochemical couples for advanced rechargeable batteries, improvements in battery and fuel-cell materials, and establishment of engineering principles applicable to electrochemical energy storage and conversion. Major emphasis is on applied research that will add to superior performance and lower life-cycle costs.

Chemical applications research includes topics such as separations, catalysis, fuels, and chemical analyses. Included in this program area are projects to develop improved, energy-efficient methods for processing product and waste streams from synfuel plants, coal gasifiers, and biomass conversion processes. Of particular interest are new techniques to remove compounds such as H_2S, NH_3, and phenols from effluents, and to devise energy-efficient means for product recovery. Also of current interest are the development of advanced methods for production of alcohols from hydrocarbon fuels, and the use of organometallic catalysts to promote the hydrogenation of coal compounds.

X-ray absorption spectroscopy is being used to characterize both organic and inorganic materials, and ultrasensitive spectroscopies are being adapted for chemical analyses of trace amounts of rare-earth and actinide compounds.

Materials applications research includes evaluation of the properties of advanced materials, as well as development of novel preparation techniques. For example, techniques such as sputtering, laser ablation, and pulsed laser deposition are being used to produce high-temperature superconducting films. Other projects include development of sol-gel and solvent-extraction methods to produce aerogel superinsulators; use of gas-particle suspensions for direct solar-thermal conversion processes and for catalysis of important thermochemical reactions; and development of light-scattering techniques to characterize biological systems.

Program Staff

Elton J. Cairns, *Program Leader*
Richard E. Russo, *Deputy Program Leader*

Nicolas Barthelemy
Paul Berdahl
Rosemary Bittmann
Harvey Blanch
Gessie Brisard
Robert Broekhuis
Garth Burns
Wanqing Cao
Van Carey
Wing-Tat Chan
Ernest Chen
Jenn-Shing Chen
Jie Chen
Yohan Choi
Tina Chow
Douglas Clark
Christopher Coen
Stephen Cramer
A. Louise Creagh
Laurent Fenouil
Richard Fish
Albert Flounders
Hubert Gasteiger
Melissa Grush
Gregory Hiller
Arlon Hunt
Mary Hunt
Caryn Jantzen
Jordan Kahn
Marvin Kilgo
C. Judson King III
Kimio Kinoshita
Judith Klinman
Gregory Klunder
David Koch
Karen Koigawachi
Fanping Kong
Susan Lauer
Jane Lee
Yongsik Lee
Scott Lynn
Anthony Mancuso
Xianglei Mao
Frank McLarnon
Douglas Miller
Kenneth Miller
Juleh Minoo
Jeffrey Moore
Stuart Naftel
Robert Plivelich
Bruch Rauhe
Ronald Reade
Paul Ridgway
James Rudnicki
Richard Russo
David Shurig
Robert Selleck
Mark Shannon
Daniel Shapiro
David Smith
Jonathan Spear
Charlotte Standish
Kathryn Striebel
Jerome Thomas
Gavin Towler
Lisa Tung
Jan van Elp
Jean-Marie Walker
Xin Wang
Charles Wilke
Richard Williams
David Wruck
Mark Yahnke
Souquan Zeng
Sheng-Tao Zhang

Electrochemistry

Exploratory Technology Research Program for Electrochemical Energy Storage

Lawrence Berkeley Laboratory is the lead center for management of the Exploratory Technology Research (ETR) Program, which is supported by the Electric/Hybrid Propulsion Division of DOE's Office of Transportation Technologies. The program's research supports DOE development of electrochemical energy conversion systems for potential use in electric vehicles. The most promising electrochemical technologies are identified and transferred to industry and/or to another DOE program for further development and scale-up.

The ETR Program identifies new electrochemical couples for advanced batteries, determines the technical feasibility of the new couples, improves battery components and materials, establishes engineering principles applicable to electrochemical energy storage and conversion, and investigates fuel cell and metal/air systems for transportation applications. Major emphasis is given to applied research that will lead to superior performance and lower life-cycle costs.

The LBL senior investigators participating in the project are E.J. Cairns, K. Kinoshita, and F.R. McLarnon of the Energy and Environment Division; and L.C. DeJonghe, J.W. Evans, R.H. Muller, J.S. Newman, P.N. Ross, and C.W. Tobias of the Materials Sciences Division. Research projects conducted by subcontractors are described in the annual report *Exploratory Technology Research Program for Electrochemical Energy Storage* (LBL-32212); LBL in-house work is summarized below. Highlights of the subcontracted work follow.

Exploratory Research

Projects to develop rechargeable conducting-polymer cells were conducted and completed at the University of Pennsylvania and SRI International. Researchers at the University of Pennsylvania used radiation-polymerization to produce polymer electrolytes from various oligomers that contain different compositions of plasticizer (ethylene carbonate and propylene carbonate) and 1 M $LiAsF_6$. Polymer electrolytes with ≥50 wt% propylene carbonate in mixtures with ethylene carbonate exhibit electrochemical properties (reversible Li redox process) and physicochemical properties (ionic conductivity $>8 \times 10^{-4}$ ohm^{-1} cm^{-1} at room temperature, glass-transition temperature of -94°C, amorphous structure from -90 to 150°C) acceptable for use in rechargeable Li cells. SRI International has developed a Li-ion conducting PEO-type polymer in which oxygen is replaced by sulfur. The best-performing polymer electrolyte, obtained from sulfur-substituted PEO (16.7 wt% S) and tetraethylorthosilicate with a plasticizer, exhibited a conductivity of 7.5×10^{-4} ohm^{-1} cm^{-1} in a Li/Li cell.

Acme Electric was recently selected to evaluate LBL-developed electrolyte compositions in Zn/NiOOH cells and to demonstrate long cycle life. The intent of this subcontract is to assist an industrial company to develop a technology base to manufacture Zn/NiOOH cells for electric-vehicle applications.

Applied Science Research

Research projects at the Illinois Institute of Technology (IIT) and the Environmental Research Institute of Michigan (ERIM) are underway to develop corrosion-resistant coatings for high-temperature batteries. IIT observed that complete removal of moisture from the electrolysis bath is necessary to obtain reproducible, high-quality electrodeposited Mo_2C coatings. A new project at ERIM is evaluating TiN-coated containment materials in Na/S cells. In preliminary studies at Ford Motor Company, sputter-coated TiN on Al resisted attack for 72 hours in a polysulfide melt. A reactive-sputtering system is being assembled at ERIM to duplicate the quality of the coatings obtained at Ford and to evaluate the corrosion-resistant properties of TiN for extended periods in polysulfide melts.

Brookhaven National Laboratory has used extended x-ray absorption fine structure and x-ray absorption near-edge spectroscopy to study mossy Zn deposits that form in alkaline zincate electrolytes. The Zn deposited at -65 mV (*vs.* Zn wire reference electrode) is oriented with the c-axis parallel to the lines of current, whereas the deposit at -45 mV has a random orientation like that of a Zn foil.

Case Western Reserve University used *in situ* spectroscopic techniques and thermal analysis to study the Li/organic electrolyte and Li/poly(ethylene oxide) interfaces. Interactions between Li and tetrahydrofuran, and the formation of LiO and $LiCO_3$ species, were detected. Preliminary cyclic voltammetry studies of Au in contact with $LiClO_4$ poly(ethylene oxide) electrolyte at 55°C showed evidence for underpotential deposition of Li.

Jackson State University evaluated the electrochemical properties of the C_{60} fullerene as an electrode material that may be useful in rechargeable Li cells. The cyclic voltammograms of C_{60} in $LiClO_4$/polyethylene glycol 400 dimethyl ether (PEG400DME) indicated five redox peaks which suggested the formation of C_{60}^{-}, C_{60}^{2-}, C_{60}^{3-}, C_{60}^{4-} and C_{60}^{5-}. These anions dissolve in PEG400DME.

Johns Hopkins University observed that iron and 1018 carbon steel display an extensive and stable passive region in $LiAsF_6$/dimethoxyethane. In a nominally dry $LiAsF_6$/DME solution (<100 ppm H_2O), the breakdown potentials of iron and carbon steel are 1300 mV (*vs.* saturated calomel electrode) and 1050 mV, respectively. The adsorption of $LiAsF_6$/dimethoxyethane and the formation of carbon-based polymer film are believed to be responsible for passivation.

Air Systems Research

Researchers at Case Western Reserve University have observed that the catalytic activity for the reduction of O_2 at

cobalt tetrasulfonated phthalocyanine (CoTsPc) adsorbed on ordinary pyrolytic graphite (OPG) in alkaline solution is enhanced by ~60 mV in the presence of alcohols. Further, the presence of methanol has no short-term deleterious effect on the kinetics for O_2 reduction on CoTsPc/OPG, which also exhibits negligible catalytic activity for methanol oxidation.

A program was initiated at Eltech Research Corporation to investigate the viability of graphitized carbon blacks and metal oxides as electrocatalyst supports in bifunctional air electrodes for electrically rechargeable Zn/air cells. Graphitized carbon blacks of Monarch 120 and Shawinigan acetylene black, and the metal oxides of $NiCo_2O_4$, Co_3O_4, $Pb_2Ru_2O_7$ and $Pb_2Ir_2O_7$ have been prepared. Electrochemical tests are underway in small cells at Metal Air Technology Systems International, Inc.

Los Alamos National Laboratory has found that processing membrane-electrode assemblies (MEA) with membranes that contain the Na^+ form rather than the H^+ form permits use of higher processing temperatures—185 *vs.* 135°C. These MEA are more robust, have a lower impedance, and are more tolerant to adverse humidification conditions in fuel cells. Measurements of some of the H_2O-management properties of Nafion 117, membrane C, and an experimental Dow membrane showed that the Dow membrane appears to have the highest H_2O uptake and smallest water drag. A large 50-cm^2 cell was operated which attained an initial performance of 2 A/cm^2 on O_2 (5 atm) without experiencing transport losses at the O_2 electrode. The initial performance on air (5 atm) showed only marginal losses up to 1 A/cm^2.

BNL utilized x-ray absorption spectroscopy to investigate the properties of Pt/C and several of its alloys with Cr, Co and Ni. The results indicate that alloying with Ni has a large effect on the d character of Pt, whereas Cr has little effect. Nickel forms a solid solution with Pt, with the Ni atoms substituting at Pt sites. Our subcontracts with the Illinois Institute of Technology, Jackson State University, and Case Western Reserve University (Electrocatalysts for Oxygen Reduction) have been completed.

Future Directions

LBL has signed a Cooperative Research and Development Agreement with the United States Advanced Battery Consortium to develop advanced batteries for electric vehicles. Several principal investigators involved in the ETR Program will work with the Consortium to develop Li/polymer-electrolyte batteries.

References

Kinoshita K, *et al.* Exploratory technology research program for electrochemical energy storage—annual report for 1991. Lawrence Berkeley Laboratory Report No. LBL-32212, June 1992.

Kinoshita K. *Electrochemical Oxygen Technology*. John Wiley, New York, 1992.

Kinoshita K. Characterization of nonaqueous lithium. *Preprints of the Annual Automotive Technology Development Contractors' Coordination Meeting*, Volume II, Dearborn, MI, November 1992.

Investigators

E.J. Cairns
K. Kinoshita
F.R. McLarnon

Advanced Electrode Research

We have been studying the behavior of electrodes used in advanced secondary batteries and fuel cells currently under development for energy storage applications. In addition, we have been investigating practical means for improving the performance and lifetimes of these batteries and fuel cells. Systems of current interest include ambient-temperature, alkaline-electrolyte rechargeable cells with Zn electrodes (Zn/NiOOH, Zn/air); rechargeable high-temperature cells (Na/S, LiAl/FeS_2); and fuel cells. We study life-limiting and performance-limiting phenomena under realistic cell operating conditions.

Evaluation of Sodium/Sulfur-Phosphorus Cells

The high-temperature Na/S cell offers very good performance, and recent improvements to the process for manufacturing the ceramic β"-Al_2O_3 electrolytes indicate that acceptable cell lifetimes may be realized. However, the Na/S "battery" performance is below that which is expected for a high-temperature (350°C) system, and electrode structures must be improved. The addition of phosphorus to the sulfur electrode is expected to result in improved specific energy because of the low equivalent weight of phosphorus.

Phosphorus-sulfur ratios of 0.143, 0.332, and 1.17 were investigated. The best cell performance was obtained with a P/S composition ratio of 0.143 in the positive electrode. Compared with Na/S cells, this composition gave higher cell voltages, leading to calculation of a theoretical specific energy 11% higher than that of the Na/S cell. Polarization measurements showed the phosphorus additive to reduce cell performance under restricted experimental conditions.

Equilibrium cell EMF data from experiments using P/S ratios of 0.143 and 0.332, along with published data, were used to infer some aspects of the phase equilibria of the Na-P-S ternary system at 350 and 400°C. The studied region was the sulfur-rich corner of the ternary diagram extending to a Na mole fraction of 0.4 and a phosphorus mole-fraction of 0.25. At least three three-phase regions appear to exist. We developed phase diagrams consistent with the experimental and published data and which can be used to further clarify the phase equilibria of this little-studied system.

Effect of Electrocatalyst and Electrolyte Composition on Methanol/Air Fuel Cell Performance

Because fuel cells promise higher energy-conversion efficiency and lower emissions than are produced by combustion engines, fuel cells are being developed for use in electric vehicles. Present-day fuel cells operate on H_2; therefore either a H_2 storage device or a reformer must be carried aboard the vehicle—resulting in a heavy, bulky, complex fuel-cell power plant. There is a strong need to develop a fuel cell that can electrochemically oxidize liquid fuels, and the successful development of a direct-methanol fuel cell (DMFC) would represent a major advance for

fuel-cell-powered vehicles.

Model fuel-cell experiments using a Pt-Ru catalyst supported on graphitized carbon have demonstrated a marked increase in performance over supported Pt for oxidation of CH_3OH in concentrated Cs_2CO_3 electrolytes. The performance curves for Pt-Ru at 120°C shown in Fig. 1 (a plot based on mg of total metal) match or exceed performance reported by others on Pt-black or supported Pt in concentrated Cs_2CO_3 at 120 to 150°C, and on supported Pt-Ru in concentrated H_3PO_4 at 200°C. These performance results were higher than any reported in the literature.

In experiments performed to evaluate the effect of various polytetrafluoroethylene (PTFE) content levels in the porous-electrode reaction layer, maximized performance was found at 20-30 wt% PTFE. Similar experiments to evaluate the effect of temperature indicated that performance was maximized at 10 to 15°C below the boiling point of the electrolyte. The decrease in performance as the temperature approaches the boiling point of the electrolyte is attributed to an increase in the water vapor pressure, which inhibits diffusion of the fuel and reaction products in the gas phase.

Future tests will monitor the composition of the fuel outlet gases to determine whether the CH_3OH oxidizes completely to CO_2, and to identify parameter values that may maximize fuel conversion efficiency. Also, the composition of the catalyst (a 1:1 Pt:Ru atomic ratio has been used so far) may be further optimized.

Methanol Electrooxidation on Well-Characterized Platinum-Ruthenium Alloys

Implementation of a practical DMFC has been prevented by poor understanding of the deactivation processes that occur on the CH_3OH anode catalyst, and considerable research has been directed toward finding novel catalyst materials. The most active catalysts known today are alloys of Pt and Ru, whose electrochemical performance has been characterized intensively, including application on carbon-supported high-surface-area fuel-cell electrodes. Although Pt-Ru electrode performance is superior to that of Pt electrodes, deactivation nevertheless occurs. Improvements in anode performance demand that the Pt-Ru surface electrocatalysis be understood on a fundamental level.

The method used to prepare of carbon-supported electrodes (*i.e.*, heating in H_2, N_2 or air) reportedly has a major effect on electrode performance. Atomically resolved surface characterization is necessary to investigate these effects and can be achieved by using ultra-high-vacuum (UHV) techniques such as Auger electron spectroscopy (AES), x-ray photoelectron spectroscopy (XPS) and low-energy ion scattering (LEIS). For this purpose, we carried out research on smooth, polycrystalline Pt-Ru alloys of various compositions, enabling us to assess the chemical state of the alloys (oxide *vs.* metal) and their surface composition prior to electrochemical measurements, while maintaining atomically flat surfaces.

Our UHV analysis has established that annealing of Pt-Ru alloys in UHV or in H_2 produces surfaces strongly enriched in Pt. A similar phenomenon can be expected for carbon-supported catalysts, and the commonly reported optimum catalyst composition of 50% is likely to have a Pt-enriched surface. The electrochemical characterization of O_2-free Pt-Ru alloys in our laboratory was carried out by means of cyclic voltammetry and potential-step experiments in the presence of CH_3OH at 25°C in H_2SO_4 (Fig. 2, next page). Whereas Pt showed superior electrocatalytic activity for fresh (unused) electrodes, prolonged CH_3OH oxidation deteriorated its activity; alloys with small amounts of Ru on the surface gave significantly better performance after a short time. Compared with Pt, an alloy containing 10% Ru on the surface enhances oxidation of CH_3OH by a factor of 30; an alloy with a Ru surface concentration of 50% improves the activity of pure Pt by a factor of 10. This result contrasts with

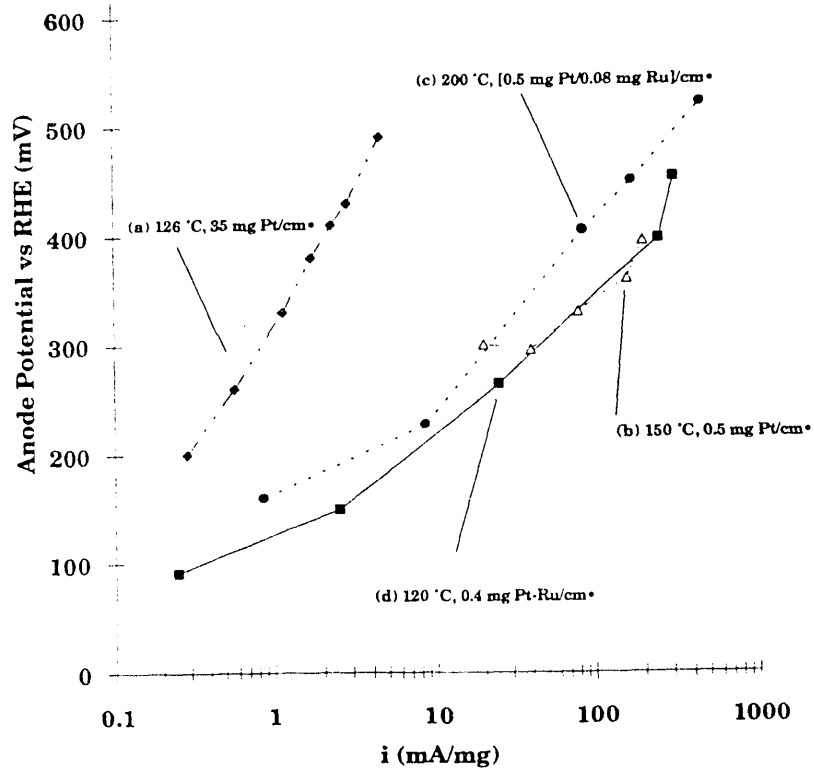

Figure 1.

Performance of LBL fuel cell anode vs. literature reports. (a) Cairns et al, *concentrated Cs_2CO_3 electrolyte; (b) Giner* et al, *concentrated Cs_2CO_3 electrolyte, Pt supported on carbon; (c) Landsman* et al, *concentrated H_3PO_4 electrolyte, Pt-Ru on carbon; (d) LBL, concentrated Cs_2CO_3 electrolyte, Pt-Ru on graphitized carbon.*

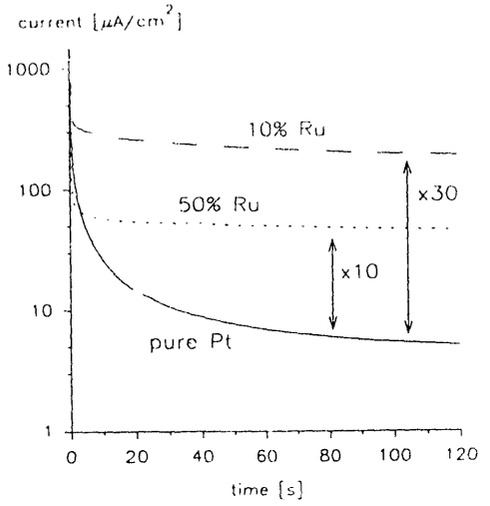

Figure 2.
Electrooxidation results show potentiostatic CH_3OH oxidation currents at +500 mV vs RHE of Pt-Ru alloys of differing surface concentrations. Experimental electrolyte: 0.5 M H_2SO_4, 0.5 M CH_3OH added, +50 mV polarization, 25°C.

previous reports claiming an optimum alloy composition of 50% Ru.

Our results give important new insight into the catalytic mechanism occurring on Pt-Ru alloy surfaces. The high catalytic activity of small amounts of Ru indicate the high surface mobility of surface-bound CO, whose further oxidation probably proceeds on Ru sites, whereas the adsorption of CH_3OH occurs exclusively on Pt atoms. Methanol adsorption (especially at the low methanol concentrations envisaged in a DMFC) is a slow, often rate-limiting step which therefore requires an even larger surface concentration of Pt. This was also confirmed in our experiments using 0.005 M CH_3OH solutions. The implication for carbon-supported alloy electrodes is that catalysts containing low concentrations of Ru should be investigated to possibly attain better DMFC performance.

Poisoning of Platinum Electrocatalyst Surfaces: NMR Spectroscopic Studies

Platinum is the most active single-component catalyst for methanol electrooxidation in DMFCs; however, poisoning reactions at the surface render the electrode ineffective under target operating conditions. Recently, a number of *in situ*, online, and *ex situ* techniques have sought information on the nature of the poisoning intermediate(s) in this system. Significant advances have been made toward this end, although no current technique can yield information on practical (supported, dispersed) electrocatalysts via *in situ* analysis.

Nuclear magnetic resonance (NMR) spectroscopy is a quantitative, nondestructive method of probing the chemical environment of a specific nucleus and has been used successfully in catalysis and surface science as a tool for identifying chemisorbed species. Because it is a bulk technique, NMR has been applied to systems very similar to practical catalysts. Our research seeks to extend the application of NMR spectroscopy in order to obtain information on surface poisoning of graphite-supported platinum DMFC anodes in H_2SO_4 electrolyte containing CH_3OH.

Carbon monoxide has been postulated as the main poisoning adsorbate in the CH_3OH electrooxidation reaction, as suggested by *in situ* reflectance IR studies on smooth Pt electrodes. Our preliminary studies therefore concentrate on a model system of adsorbed CO. We have built and tested a probe for observation of ^{13}C magnetization, and work on the model system is currently underway.

Investigations of Methods to Improve the Lifetime of the Zinc/Nickel Oxide Cell

Rechargeable alkaline Zn/NiOOH cells can be designed to deliver high specific energy and specific power, but their short lifetimes have precluded commercial acceptance. The high solubility of Zn species in alkaline electrolytes tends to enhance undesirable physicochemical processes such as active material redistribution (shape change) and filamentary Zn growths (dendrites) that degrade cell capacity and limit cell life.

Our earlier work demonstrated that KOH-KF, KOH-K_2CO_3 and KOH-KF-K_2CO_3 electrolytes can greatly extend the cycle life of 1.35-Ah Zn/NiOOH cells. The KOH concentration in these new electrolytes is about half of that used in previous versions of Zn/NiOOH cells, which results in a fivefold reduction in Znspecies solubility. The rate of Zn-electrode shape change is much slower in these cells, and cell cycle life can be increased to 450-800 deep-discharge cycles (which may be compared to 100-200 cycles in KOH electrolyte) (Fig. 3). When the new electrolytes are used, the final cell capacity is limited by the NiOOH electrode, and the Zn electrode shows only a modest extent of shape change.

We have recently focused our efforts on developing methods to improve the NiOOH electrode capacity retention in these electrolytes. Our experiments illustrate how the amount of active material loaded into the pores of the NiOOH electrode substrate affect cycle-life performance of the electrode. Using various electrolytes (Fig. 3), sealed 1.35-Ah Zn/NiOOH cells containing NiOOH electrodes loaded at 1.6 g/cm^3 void space failed within 150 deep-discharge cycles. The Zn electrodes in these cells showed little shape change, but the NiOOH electrodes exhibited poor coulombic efficiency. This result contrasted markedly with the long-lived cells noted above, which used NiOOH electrodes loaded at 1.3 g/cm^3 void space.

In another experiment, two Zn/NiOOH cells were constructed in an identical manner, except that Cell A had NiOOH electrodes with 1.3 g/cm^3 void space, and Cell B had NiOOH electrodes with 1.6 g/cm^3 void space. Both cells contained the same KOH-KF-K_2CO_3 electrolyte and were sealed under vacuum in a starved-electrolyte condition. The capacity of both cells declined after about 125 deep-discharge cycles, at which time the the cell seals were broken and a regeneration cycle (slow discharge to zero cell voltage, and a slow overcharge to twice the NiOOH electrode capacity) was applied. A small amount of electrolyte was then added to each cell, and the cells were resealed at 0.5 bar instead of full vacuum. Both cells showed dramatic recovery of their capacities. Cell A retained 90% of its initial capacity after 340 cycles, maintained 95% coulombic efficiency, and *in situ* x-ray images

showed almost no Zn-electrode shape change. Cell A delivered 300 W/kg peak specific power at 0% depth of discharge (DOD), and 170 W/kg at 80% DOD. At cycle 210, cell B retained 80% of its initial capacity, but its coulombic efficiency declined to 90%. Several new NiOOH electrode materials, including new lightweight fiber-based types, are currently under investigation.

Investigation of Zinc Species Precipitation in Nickel Electrodes

Our recent improvements in the performance of the Zn electrode in Zn/NiOOH cells have shown that NiOOH limits the lifetime of this cell. A possible mechanism for this degradation of NiOOH-electrode capacity is the precipitation of inorganic nickel-zinc salts, which may passivate the electrode. *Ex situ* spectroscopic data are being gathered to identify species possibly present. Based on this information, a reasonable strategy for improving the NiOOH positive electrode may be formulated.

We have used x-ray diffraction to examine NiOOH electrodes cycled in Zn/NiOOH cells. The resultant data have not been conclusive, however, perhaps because of a lack of long-range order in the NiOOH electrode. To overcome this problem, other *ex situ* spectroscopic methods are being evaluated to identify any such passivating species.

Vibrational spectroscopy includes both Raman spectroscopy and infrared (IR) spectroscopy. Both methods provide information on the nature of chemical bonding and can also be used quantitatively. IR spectroscopy of solid phases, however, is dependent on the method of sample preparation. In our experiments, the Ni sinter was magnetically separated from the active material (*e.g.*, Ni(OH)$_2$ and NiOOH) and a CsI mull was prepared. The resulting spectra were of only fair quality, probably because of optical limitations of the available equipment (Analect Model RFX-30 FT-IR). Raman spectroscopy is more flexible with respect to sample preparation and appears to offer better prospects for acquiring useful spectra.

X-ray Photoelectron Spectroscopy (XPS) can provide information about the oxidation states of elements within an electrode. The sensitivity of XPS is roughly uniform for most elements (*i.e.*, sensitivity approximately 0.1 mol%), and the technique has been extensively represented in the literature. An important disadvantage of XPS is the need to maintain UHV over the sample during the measurement. Because considerable evidence indicates the presence of intercalated H_2O between Ni(OH)$_2$ "sheets" in the NiOOH electrode, UHV may be difficult to attain. However, various sample pretreatment methods (*e.g.*, gentle heating under vacuum) may mitigate this problem. Another difficulty lies in the surface-sensitive nature of XPS. Species found on the electrode surface may be a result of side reactions occurring during cell operation, or may arise during sample preparation, and may not be representative of the electrode composition during or immediately after cycling.

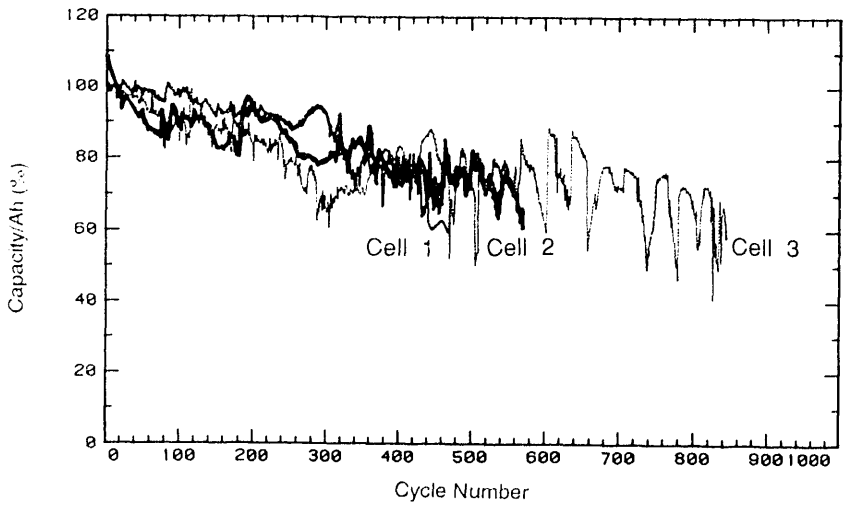

Figure 3.

Capacity retention of 1.35-Ah Zn/NiOOH cells with various electrolytes. Cell 1: 2.5M KOH, 2.5M K$_2$CO$_3$, 0.5M LiOH; Cell 2: 3.2M KOH, 1.8M KF, 1.8M K$_2$CO$_3$; Cell 3: 3.5M KOH, 3.3M KF.

References

Adler TC, McLarnon FR, Cairns EJ. Low-zincate-solubility electrolytes for use in zinc/nickel oxide cells. *J. Electrochem. Soc.* 1993; 140: 289.

Cairns EJ, Adler TC, McLarnon FR. New electrolytes for long-lived zinc electrodes. Paper No. IL-4-20 presented at the 43rd Meeting of the International Society of Electrochemistry, Cordoba, Argentina, 1992.

Jain R, Adler TC, McLarnon FR, Cairns EJ. Development of long-lived high-performance zinc-calcium/nickel oxide cells. *J. Appl. Electrochem.* 1992; 22: 1039.

Cairns EJ, Ridgway PL, McLarnon FR. EMF measurements of the Na/Na$_2$P$_4$S$_5$ cell. Paper presented at the 182nd Electrochemical Society Meeting, Toronto, Canada, 1992.

Lessner PM, McLarnon FR, Winnick J, Cairns EJ. Aqueous polysulfide flow-through electrodes: effects of electrocatalyst and electrolyte composition on performance. *J. Appl. Electrochem.* 1992; 22: 927.

Rudnicki JD, McLarnon FR, Cairns EJ. *Application of Photothermal Deflection Spectroscopy to Electrochemical Interfaces.* Lawrence Berkeley Laboratory Report No. LBL-32127, March 1992.

Gasteiger HA, Cairns EJ, Ross PN, Markovic N. Well-characterized Pt-Ru alloys for methanol oxidation. Paper presented at the 182nd Electrochemical Society Meeting, Toronto, Canada, 1992.

Investigators

E.J. Cairns — *J.A. Reimer**

F.R. McLarnon — *R.F. Plivelich*

T.C. Adler — *P.L. Ridgway*

H.A. Gasteiger — *P.N. Ross**

M.S. Yahnke

*Materials Sciences Division, LBL.

Advanced Rechargeable Zinc Cells

Zinc is the most commonly used battery electrode because of its low equilibrium potential, electrochemical reversibility, compatibility with aqueous electrolytes, low equivalent weight, high specific energy and volumetric energy density, abundance, low cost, low toxicity, and ease of handling. Zinc has been considered for use as the negative active material in several rechargeable batteries; however, short lifetimes have severely limited the use of such batteries. LBL research has produced major improvements in the lifetime of the rechargeable Zn electrode in alkaline electrolytes, and efforts are under way to apply these improvements to rechargeable Zn/air and Zn/NiOOH cells.

Development of 20-Ah Zinc/Nickel Oxide Cells

A 20-Ah Zn/NiOOH cell was constructed using NiOOH electrodes with an active material loading of 1.6 g/cm^3 void space. The dimensions of the Zn and NiOOH electrodes were 15 cm × 15 cm, approximately the size that would be used in electric-vehicle batteries. The cell contained KOH-KF-K_2CO_3 electrolyte and was sealed under a vacuum. A small piece of Pt catalyst material was used to oxidize the small amount of H_2 gas liberated by the Zn electrode during charge, and steady-state pressure was maintained at less than 1 bar. The internal temperature of the cell was satisfactory: it did not exceed 30°C during charge and during a one-hour 15-Ah discharge.

Cell capacity dropped below 60% of its initial value after 185 cycles at 80% depth of discharge. Capacity was limited by the NiOOH electrode, and an *in situ* x-ray image of the Zn electrode showed little shape change. Another 20 Ah-cell will be constructed using NiOOH electrodes with a loading of 1.3 g/cm^3 and will be pressurized for improved wetting characteristics. Acme Advanced Energy Systems (Tempe, AZ) is developing the Zn/NiOOH battery for electric vehicle applications under a subcontract with LBL, which is cooperating with Acme to transfer this promising technology.

Development of Electrically Rechargeable Zinc/Air Cells

The primary life-limiting component of electrically rechargeable zinc/air cells is the bifunctional air electrode. Perovskites, pyrochlores and spinel oxides have been suggested as bifunctional air electrocatalysts, *i.e.*, catalyst of O_2 reduction (during discharge) and H_2O oxidation to O_2 (during charge). Because the perovskite $La_{0.6}Ca_{0.4}CoO_3$ exhibits current densities as high as 3 A/cm^2 when combined with a high-surface-area carbon in a gas-diffusion electrode (Shimizu et al., *J. Electrochem. Soc.* 1990; 137: 3430), our preparation and study of bifunctional air electrodes have focused on this electrocatalyst.

Several techniques for preparing of phase-pure $La_{0.6}Ca_{0.4}CoO_3$ powder with a high specific surface area and small, uniform particle size distribution were evaluated. The amorphous citrate precursor method yielded fairly pure powders with limited crystallinity and Brunauer-Emmett-Teller (BET) surface areas up to 18 m^2/g. A modification of this procedure, called the Pechini process, improved the particle size uniformity but resulted in smaller specific surface areas. An alternate procedure (the glycine nitrate combustion method, which involves rapid combustion of a stoichiometric mixture of metal nitrates with glycine fuel) led to more uniform, but porous particles without improving the specific surface area.

In our procedure for producing gas diffusion electrodes, gas supply and active layers were prepared by dispersion of PTFE-containing mixtures of graphitized carbon (and catalyst for the active layer) with acetone, followed by kneading and rolling. The two layers were then rolled together with a Ni screen current collector, then dried and pressed at 340°C to sinter the PTFE. Variations in the procedure were evaluated by testing 1-cm^2 electrodes in a three-electrode cell. Larger (25 cm^2) electrodes were cycled in 0.9-Ah cells with reticulated flow-through, soluble Zn electrodes, and an electrolyte composition of 45 wt% KOH and 40 g Zn^{2+}/l. The perovskite-catalyzed electrode (Figure) achieved 45 cycles (to a cell cutoff voltage of 1 volt), which may be compared with a macrocycle-catalyzed commercial electrode from Electromedia Co. that attained 72 cycles (C/6 charge rate, C/3 discharge rate). A key factor in the failure of these 0.9-Ah cells may be flooding of the air electrode, which is probably associated with the electrolyte carbonation caused by incomplete scrubbing of the inlet air. However, declining performance due to catalyst degradation cannot be ruled out. Other techniques for evaluating the performance and stability of transition-metal oxide electrocatalysts, such as cyclic voltammetry and measurements on oxide/carbon pastes in recessed disk electrodes, are under development.

The pulsed laser deposition technique (laser ablation) has been used to prepare a thin film of $La_{0.6}Ca_{0.4}CoO_3$ on a glassy carbon substrate, which was then made into a rotating disk electrode. This approach should enable measurements of O_2 reduction (OR) and O_2

evolution (OE) kinetic rate constants for comparison with other oxides on the basis of equal catalyst/electrolyte interfacial area. Preliminary studies on this film were carried out in 0.1-6.9 M KOH electrolyte, and the results indicated reasonable stability of the oxide films towards dissolution. For OR and OE, respectively, tafel slopes of 120 and 40 mV/decade were computed from mass-transfer-corrected current measurements in 6.9 M KOH electrolyte. Scanning electron microscopy (SEM) analysis showed the film to be porous. Optimization of the deposition process to yield dense films is now underway using other substrate materials.

References

Striebel K, Muller S, McLarnon F and Cairns E. Perovskite-catalyzed bifunctional-air electrodes for Zn/air cells. Paper no. 3 presented at the 182nd Meeting of the Electrochemical Society, Toronto, Canada, 1992.

Chen JS, McLarnon FR and Cairns EJ. Investigation of low-zinc-solubility electrodes and electrolytes in zinc/silver oxide cells. *J. Power Sources* 1992; 39: 333.

Investigators

E.J. Cairns
F.R. McLarnon
K.A. Striebel
T.C. Adler
*S. Müller**

*Paul Scherrer Institut
Würenlingen, Switzerland

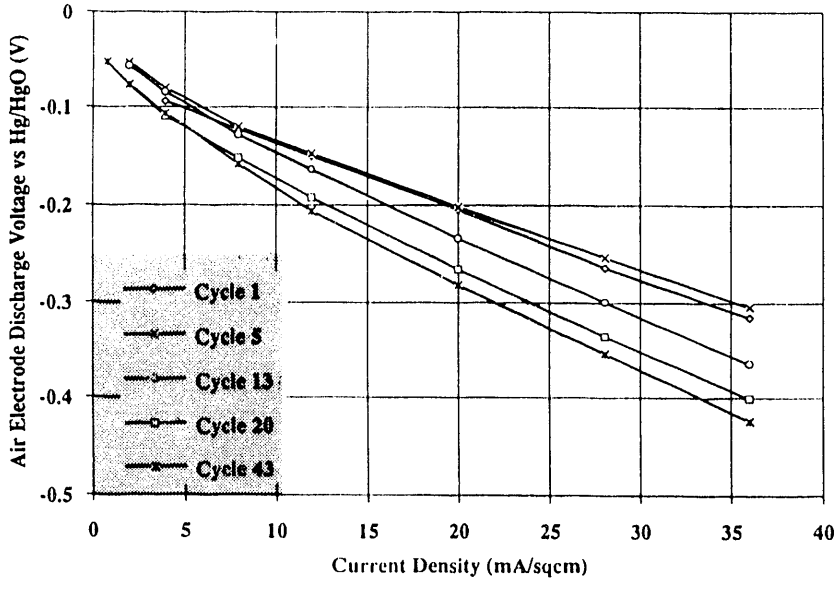

Figure.

Performance of $La_{0.6}Ca_{0.4}CoO_3$ perovskite-catalyzed air electrode during cycling in a 0.9-Ah Zn/air cell. Electrode potential is plotted as a function of current density for various cycles.

Electrode Surface Layers

We are using advanced *in situ* and *ex situ* characterization techniques to study the structure, composition and mode of formation of surface layers on electrodes used in rechargeable batteries. The primary objective of this research is to identify film properties that improve the rechargeability, cycle-life performance, specific power, specific energy, stability and energy efficiency of electrochemical cells. Earlier, we completed evaluation of ion implantation as a way to improve the corrosion resistance of lead battery electrode materials; present research focuses on transformation of surface phases that accompany the charging and discharging of Ni electrodes in alkaline electrolytes.

Effects of Foreign Cations on the Electrochemical Behavior of Nickel Oxide Electrodes

To examine the electrochemical interconversion between $Ni(OH)_2$ (the predominant species on a discharged Ni electrode) and NiOOH (the predominant species on a charged Ni electrode), and to search for an effective way to improve the utilization of active material in Ni battery electrodes, we have been studying the effects of foreign cations on the electrochemical behavior of the Ni electrode. Cobalt and Cu, two neighboring elements of Ni in the periodic table, were chosen as foreign doping elements and were introduced individually into the surface layer of the electrode by using a metal-vapor vacuum arc ion implantation technique. The energy level of the implanted ions was controlled at 50 KeV, which corresponds to a ~10-nm penetration depth of implanted ions. This depth is comparable to the actual thickness of the $Ni(OH)_2$ layer formed on Ni substrates. Because of the good match between foreign and native atom lattice constants, the foreign cations are likely to be present as substituted, rather than inserted, atoms. The ion-implanted dose level ranges from 3.2×10^{15} to 7.0×10^{16} atoms/cm^2, and the expected ratio of foreign cations to native Ni atoms is ~20% when the dose level approaches ~10^{16} atoms/cm^2.

Both cyclic voltammetric and galvanostatic charge/discharge experiments on Co-implanted Ni electrodes have demonstrated that the potentials corresponding to the transformation between NiOOH and $Ni(OH)_2$ during both oxidation and reduction processes shift toward more negative values, compared with those of Ni electrodes without doping. In addition, Co-implanted electrodes appear to have a higher coulombic storage capability. The charge quantity released from a typical Co-implanted electrode is ~20% more than that of an undoped Ni electrode. However, Cu-substituted Ni electrodes show the opposite effect.

The LBL fast spectral-scanning self-nulling ellipsometer has been used to perform *in situ* characterization of the Ni electrodes with and without foreign dopants during charge and discharge. Based on data analyses using a three-medium optical model and the effective medium theory, we have determined NiOOH volume fractions in the electrode surface layer by use of a numerical optimization process. The volume fraction of NiOOH for a co-implanted electrode with a medium dose level can reach 90-95% after charging, which may be compared to ~80% for the undoped Ni electrode (Figure). This result indicates that the transformation between $Ni(OH)_2$ and NiOOH is facilitated by the introduction of Co cations.

Copper-substituted electrodes are expected to show the opposite effect because of the different conduction mechanisms in the Ni electrode system. According to an analysis of valence states, Co and Cu dopants should function as donors and acceptors, respectively. Because NiOOH is commonly considered to be a strong n-type semiconductor, and because $Ni(OH)_2$ has poor conductivity, the introduction of donor impurities into the Ni electrode system can easily be shown to reduce the potential barriers at the boundaries between grains with different constituents and thereby promote a more complete transformation between $Ni(OH)_2$ and NiOOH. Our experimental results also support the nodular growth model proposed by Crocker and Muller.

Improved Corrosion Resistance of Lead-Acid Battery Grid Materials by Ion Implantation

Grid corrosion, particularly in the positive plate, is an important factor limiting the cycle life of lead-acid batteries. To investigate surface modification by ion implantation as a means for reducing the corrosion of grid materials. We chose 99.99% pure Pb and a Pb-4%Sb alloy as representative grid materials. Titanium was used primarily for implantation, and the implantation of several other elements produced similar results.

Two methods were employed to determine the corrosion behavior of grid materials: (i) corrosion rates were derived from the current response of the specimens in 5M H_2SO_4 electrolyte to small anodic polarization steps (3-10 mV), extrapolated from short-term measurements to zero time (in order to represent the behavior of the original surface); and (ii) the

morphology of the corroded surface after extended (60-h) open-circuit immersion in 5M H_2SO_4 electrolyte was determined by SEM examinations.

The lowest corrosion rates were obtained for the implantation of Ti into Pb and Pb-4%Sb with an energy of 60 KeV and a dose of 5.0×10^{16} atoms/cm^2. Under these conditions, the corrosion current is decreased about thirtyfold for Pb and about seventyfold for the Pb-Sb alloy. Ion implantation with V, Cr, Ni or W also improves the corrosion behavior. Depth profiles of the implanted ions were obtained by Auger spectroscopy. The profiles show a peak Ti concentration 40 nm below the surface (projected range).

References

Muller RH, Zhang S-T. Effect of ion implantation on the corrosion behavior of lead and lead-antimony alloy. Paper presented at the 182nd Meeting of the Electrochemical Society, Toronto, Canada, 1992.

Crocker RW, RH Muller. *Structural Transformation of Nickel Hydroxide Films during Anodic Oxidation.* Lawrence Berkeley Laboratory Report No. LBL-32136, 1992.

Investigators

F.R. McLarnon
*R.H. Muller**
F.-P.Kong
S.-T. Zhang

*Materials Sciences Division, LBL

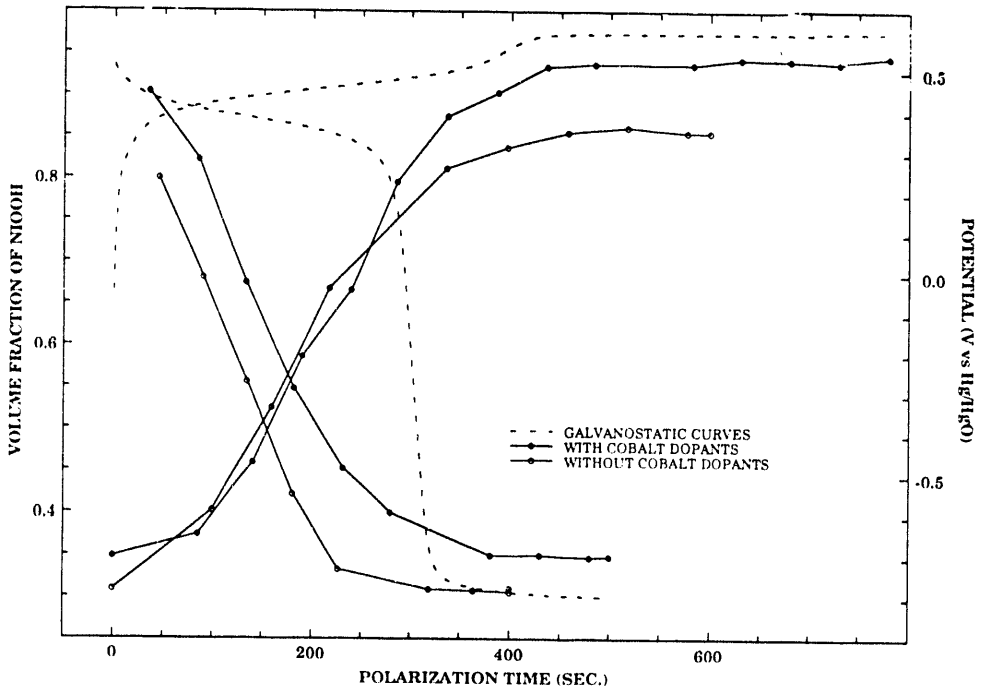

Figure.

Interconversion of NiOOH and Ni(OH)$_2$ during galvanostatic charge, and discharge of Ni electrode in 1.0 M NaOH electrolyte. Solid curves show volume fraction of NiOOH in electrode surface layer, with and without Co dopant, as determined by ellipsometric measurements. Solid curves showing increasing NiOOH content correspond to charge; solid curves showing decreasing NiOOH content correspond to discharge. Dashed curve shows Ni electrode potential vs Hg/HgO reference electrode.

Chemical Applications

Processes for High-Temperature H_2S Removal and Sulfur Recovery

This project explores the technical and economic feasibility of two high-temperature processes: one for cleaning coal gas before combustion in a gas turbine used for power production and the other a zero-emissions process for converting a mixture of hydrogen sulfide and carbon dioxide to sulfur and synthesis gas.

In the high-temperature clean-up process, the coal gas passes through a nearly isothermal, moving bed of calcium carbonate that removes particulates (by filtration), hydrogen chloride and hydrogen sulfide (by chemisorption), and ammonia (by catalysis). Our research objective is to define the temperature at which these goals can best be realized at a given pressure. Preliminary calculations indicate a probable range for this temperature of 650° to 900°C, about 100° to 500° below the outlet temperatures of most gasifiers.

Experiments on the sorption of hydrogen sulfide from gases containing carbon dioxide revealed that these two species can react, producing elemental sulfur, carbon monoxide, and hydrogen. The reaction is favored by high temperature, low pressure, and a high CO_2/H_2S ratio. Because unreacted CO_2 and H_2S can be recycled without producing a tail-gas stream, a process based on this chemistry could lead to an emission-free alternative to conventional Claus technology. We are currently determining the kinetics of the key reaction steps and evaluating the economics of such a process.

Sorption of H_2S With Limestone

The process under investigation involves removal of H_2S from the coal gas by sorption into a countercurrent moving bed of limestone particles. Theoretically, NH_3 in the coal gas is broken down by catalysis, and gasifier fines are removed by cycloning and by filtration by the moving granular bed. Our project will describe the kinetics of the reaction of H_2S with limestone and, in particular, the evolution of the solid structure during the course of the reaction using a differential quartz tube reactor. Because studies at gasification pressures would require much more expensive apparatus, our study is confined to atmospheric pressure.

The main reaction of importance in the limestone/H_2S system is:

$$CaCO_3 + H_2S \leftrightarrow CaS + H_2O + CO_2$$

which is favorable at temperatures above 807°F (704 K). The external dimensions of the solid remain constant, suggesting that the porosity of the solid increases with conversion, leading to a fast reaction and high conversion. At high temperatures and with sufficiently low fugacity of CO_2, limestone also undergoes calcination:

$$CaCO_3 + H_2S \leftrightarrow CaO + CO_2$$

The lime formed can then react with H_2S:

$$CaO + H_2S \leftrightarrow CaS + H_2O$$

In this case, however, porosity decreases on reaction and the kinetics will be slow and the conversion low.

Composition of the gas phase is dictated by the initial C:H:O ratio and the equilibrium of the water-gas shift reaction as a function of temperature:

$$CO + H_2O \leftrightarrow CO_2 + H_2$$

Failure to account for calcination and water gas shift equilibration has cast doubt on the validity of most previous studies in this system, hence this fresh evaluation of the kinetics.

Unreacted limestone. The morphology of limestone showed low porosity (less than 8%); BET analysis yielded a specific surface area ranging from 0.23 to 0.36 m^2/g with a flat distribution (average, 0.29 m^2/g). SEM pictures revealed a coarse structure with no apparent crystal.

Sintering Phenomena

Limestone. Numerous limestone samples have been heated at different temperatures for different durations under one atmosphere of carbon dioxide. Under these conditions, the calcination temperature is 892°C. In contrast to calcium oxide (lime), limestone does not sinter at a noticeable rate at temperatures up to 900°C. Pictures taken with an optical microscope (magnification between 50 and 400) confirm the absence of morphological changes on the heated limestone.

Calcium sulfide. Initial experiments with limestone sulfidation indicated a significantly reduced H_2S sorption rate after only 10-15% conversion of $CaCO_3$ to CaS. Microscopic examination of sulfided particles showed them to be much smoother than the original limestone, indicating occurrence of sintering. Reagent-grade CaS powder (average grain size 1.7 μm) heated under an atmosphere of either N_2 or H_2 at 850°C for 40 minutes produces no appreciable loss of BET surface area. However, addition of as little as 4% CO_2 to N_2 leads to significant sintering under the same conditions. In an atmosphere of 96% CO_2, 4% H_2, the CaS loses about 25% of its initial BET surface area (1.2-1.3 m^2/g) in 80 minutes at 1033K, more than 50% in the same time at 1181K.

The data for the rate of loss of surface area in this temperature range are fit reasonably well by the model of German and Munir. This model is adequate for low temperatures (750-800°C) but fails at higher values (850-900°C) for reasons that will be developed in future work.

Work will continue to determine the influence of limestone structure and composition on the kinetics sulfidation. Under some conditions an extent of sulfidation approaching 50% has been achieved, but the factors permitting this higher conversion have not been explained. The use of dolomitic limestones will also be explored. The presence of magnesia in the calcium carbonate structure may hinder the sintering of CaS and promote the diffusion of H_2S to sorption sites. Finally, because limestone is frequently mixed with the coal fed to a gasifier, use of limestone may prove advantageous for removing particulates and residual H_2S from the coal gas before it is fed to the gasifier.

Development of a Zero-Emissions Sulfur-Recovery Process

This project evolved from the experimental observation that a substantial fraction of the H_2S is converted to elemental sulfur when mixtures of CO_2 and H_2S are allowed to equilibrate at high temperatures. This process is suitable for recovery of H_2S from any acid gas stream, *e.g.*, coal gas, refinery gases or natural gas, and will provide an emissions-free alternative to the Claus process.

In the University of California Berkeley Zero-Emissions Sulfur Process (Fig. 1), H_2S and an equimolar amount of carbon dioxide are removed from the acid gas in the first absorber/stripper loop. If the acid gas contains insufficient CO_2, a make-up stream may be introduced. The CO_2/H_2S mixture is heated and enters the high temperature furnace, where a series of reactions form a mixture of CO_2, H_2S, H_2O, CO, H_2, S_2, COS, and SO_2. The distribution of sulfur among the sulfur-containing species can be found by considering the chemical equilibria:

$$H_2S \leftrightarrow H_2 + 1/2\, S_2$$

$$CO_2 + H_2 \leftrightarrow CO + H_2O$$

$$2\, CO + S_2 \leftrightarrow 2\, COS$$

$$2\, H_2S + SO_2 \leftrightarrow 3\, S + 2\, H_2O$$

This distribution varies with tempera-

Figure 1.

Schematic diagram of the University of California Berkeley Zero-Emissions Sulfur Process.

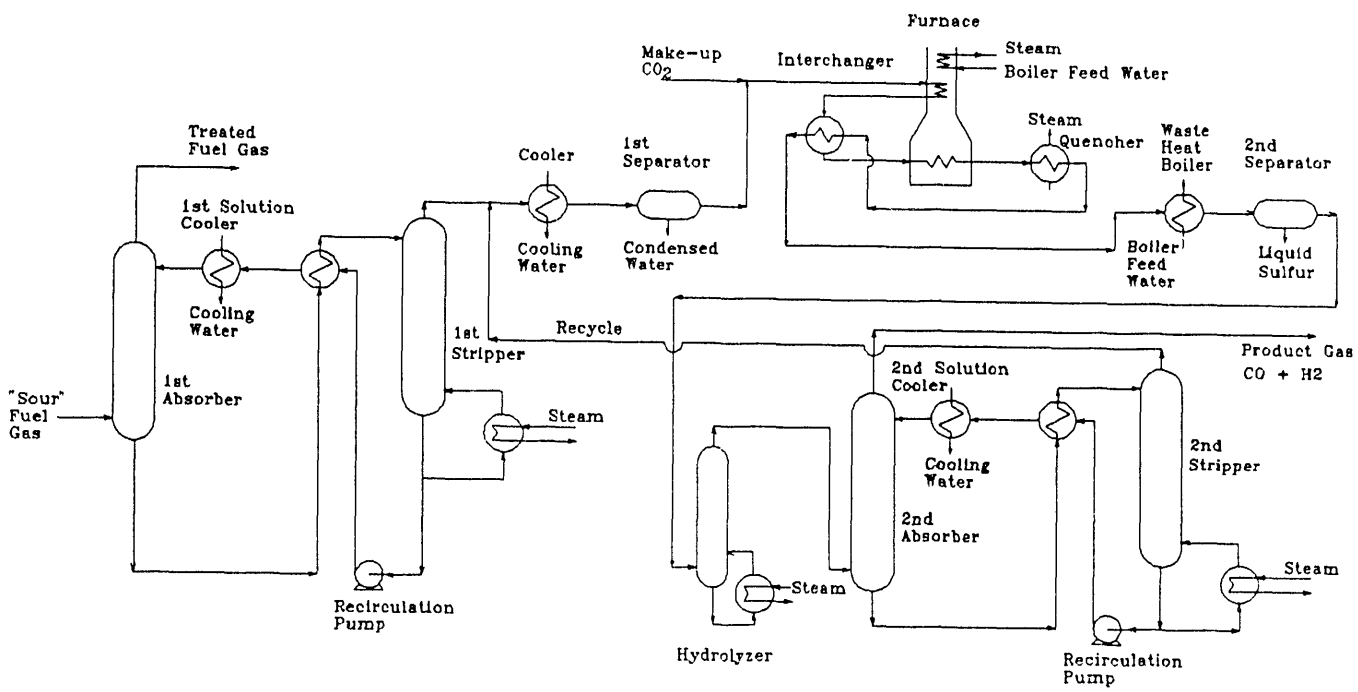

ture; formation of elemental sulfur is favored by high temperatures (Fig. 2).

Gases leaving the furnace are cooled in a series of heat exchangers that allow for recovery of heat from the hot gas. This heat is used to raise steam for the stripper and hydrolyzer reboilers. The sulfur is separated by condensation, and COS is hydrolyzed to H_2S and CO_2:

$$[COS]_{soln} + H_2O \rightarrow [CO_2]_{soln} + [H_2S]_{soln}$$

Hydrogen sulfide and carbon dioxide are then absorbed in the second absorber, leaving an essentially sulfur-free stream of carbon monoxide and hydrogen, saturated with water vapor. Hydrogen sulfide and carbon dioxide removed from the solvent in the second stripper are recycled to the reactor; therefore, emission of sulfur-containing gases to the environment is determined by the operating conditions of the second absorber and may be kept as low as is economic for the absorber design.

Thermodynamic analysis of the behavior of H_2S/CO_2 mixtures at high temperatures has shown that formation of elemental sulfur is favored by high temperature, low pressure and low amounts of water in the reactor feed (some water vapor is necessarily carried over from the first stripper). The highest fraction of elemental sulfur is formed when the reactor feed contains roughly 7% H_2S in CO_2; however, the yield-per-reactor-pass is the product of the conversion and the feed fraction, and the optimum feed ratio for the process is therefore found to be roughly 50:50 CO_2/H_2S, since this minimizes the amount of material that must be recycled.

In current experiments to identify the rate-limiting reaction in the process, the inlet gas composition, flow rate, and reactor temperature are varied. Sulfur is condensed from the outlet gas and weighed, and the composition of the remaining gases is monitored using a gas chromatograph. Formation of substantial amounts of carbonyl sulfide as a reaction byproduct can be avoided by rapid cooling. A model is being developed to describe the behavior of the experimental reactor. This model will help test theories for the reaction mechanism and may also be used for design purposes. After the identity of the rate-limiting reaction is thoroughly established, catalysts for that reaction will be investigated.

Process Evaluation. We are seeking suitable construction materials for the high-temperature furnace and are evaluating strategies for hydrolyzing byproduct COS. Use of energy within the process will be examined with a view to maximizing heat recovery. The capital and operating costs of the process will be estimated to allow a rough optimization of the process flowsheet and to permit comparison with conventional Claus technology.

Investigators

L.A. Fenouil
G.P. Towler
S. Lynn

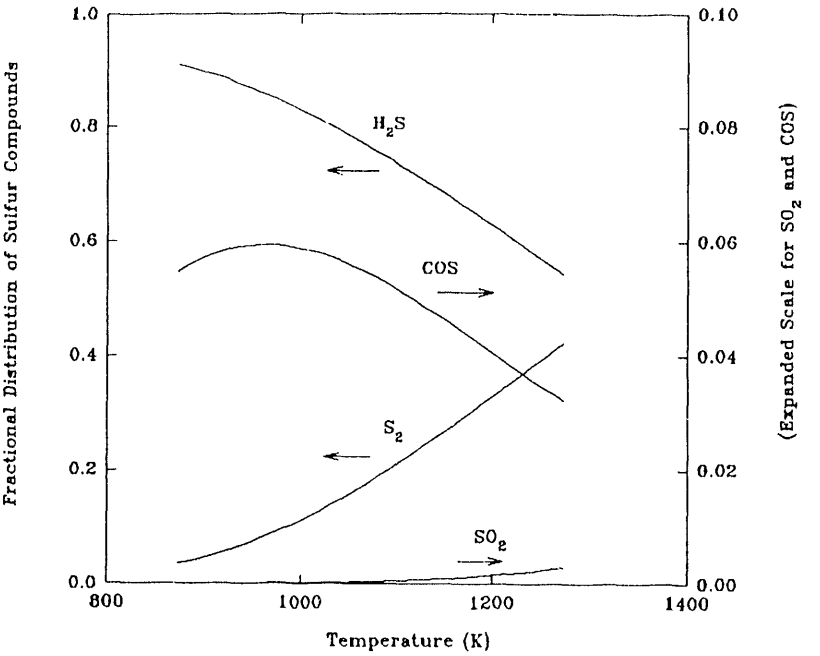

Figure 2.

Distribution of sulfur-containing species vs. temperature, at 1 atm, for a 50:50 CO_2/H_2S feed, sat. with H_2O at 40°C.

Separations by Reversible Chemical Complexation

Carboxylic acids, glycols, and related substances can be manufactured from biomass by fermentation. Some substances in this group (*e.g.*, acetic acid, ethylene, and propylene glycols) are also large-volume petrochemical products. The economics of these production processes are dominated by costs for recovery and purification of the desired product from dilute and often complex aqueous solutions. The purpose of our research is to investigate reversible chemical complexation with organic agents as a means for economical recovery of these substances. We have focused upon extraction and adsorption, although several other implementations of complexation are feasible as well.

Most of the carboxylic acids with greatest potential for economical production from biomass are relatively non-volatile dicarboxylic and hydroxycarboxylic acids. For these products, regeneration of extractants and adsorbents is challenging because distillation and other methods requiring volatility are ineffective. Glycols also have low volatilities and are difficult to separate from water because of their close similarity to it.

Recovery of Carboxylic Acids at pH > pK,1

One major complication in production of many carboxylic acids from biomass is the fact that the fermentation operates effectively only at values of pH above the pK,1 of the carboxylic acid. Under such circumstances the carboxylic acid is present largely as carboxylate anion. Extraction or adsorption can still be used for recovery of carboxylic acid products from such fermentations if extractants or sorbents with strong enough basicity are used. However, regeneration of such strongly basic extractants and sorbents is difficult.

One effective method for regenerating strongly basic extractants or sorbents is back-extraction (leaching) with an aqueous solution of trimethylamine (TMA). The resultant trimethylammonium carboxylate can be decomposed thermally to yield the product carboxylic acid and the trialkylamine for recycle.

We have sought solid sorbents and liquid extractants with an appropriately intermediate basicity such that capacity for carboxylic acids is maintained at pH > pK,1 while regeneration can be carried out using aqueous TMA. In previous batch-equilibration experiments, we demonstrated that Dowex MWA-1, a macroreticular tertiary amine sorbent (Dow Chemical Co.), has these properties for recovery of lactic and succinic acids under optimal fermentation conditions. We have now confirmed the favorable performance of this sorbent in fixed-bed studies, which show an additional useful focusing effect enhancing the concentration of the carboxylic acid in the leachate.

We have used both Alamine 336 (a mixture of trialkyl amines, Henkel Corp.) and Amberlite LA-2 (a mixture of dialkyl amines, Rohm & Haas Corp.) as extractants for lactic and succinic acids, with 1-octanol, chloroform and methyl isobutyl ketone (MiBK) as diluents. These systems give sustained capacity for solution pH two or more pH units above pK,1. Because of hydrogen bonding with the carboxylate group, 1-octanol and chloroform as diluents sustain capacity to higher pH values than does MiBK for extraction with Alamine 336, and because of additional hydrogen bonding with the additional proton of the secondary ammonium group, the capacity of Amberlite LA-2 is sustained to still higher values of pH in the presence of 1-octanol or MiBK as diluent.

For extractants as well as sorbents, regeneration would be performed by leaching with aqueous TMA. We have shown previously that regeneration and recovery of product acid are essentially complete for less soluble dicarboxylic acids, such as fumaric and succinic. However, for lactic acid it is possible to reduce the TMA level to only about 0.3 mols TMA/mol lactic acid by simple heating. Dilution of the remaining concentrate with MiBK or n-butyl acetate followed by continued heating can reduce the TMA level to 0.13 mols TMA/mol lactic acid. Essentially complete regeneration and recovery are achievable by reacting the trimethylammonium lactate with an alcohol (*e.g.*, n-butanol) to form a distillable ester (*e.g.*, n-butyl lactate).

Recovery of Diols by Complexation

Strong complexes with alcohols or diols (glycols) are difficult to form in aqueous solution because of the similarity of the hydroxyl group to water. However, one effective complexant for cis-vicinal diols is the boronate anion, which forms a ring structure with the diol. We have used 3-nitrophenyl boronic acid (NPBA) as an available organoboronate with low water solubility and with sufficient acidity to ionize and form complexes at pH down to 5.0. NPBA is paired with an organic cation, trioctylmethylammonium (TOMA), and is used with 2-ethylhexanol as diluent in a mixed solvent. During the past year we extended earlier experiments to measure and interpret chemically the extents of extraction of 1,2-propanediol, glycerol, sorbitol, fructose and lactic acid from water into this ion-pair solvent.

Phenols also hydrogen bond with alcohols and glycols. We have therefore also measured the capacity of Amberlite 761 (Rohm & Haas Corp.), a macroreticular phenol-formaldehyde resin with phenol functionality, for uptake of 1,2-propanediol (propylene glycol) from aqueous solution at 25°C and 45°C. Capacities in equilibrium with aqueous weight fractions up to 10% remain substantially less than the measured density of phenol groups on the resin, a result indicative of complexation insufficiently strong to be the basis of an attractive recovery process.

We are currently examining properties of phenol-alcohol solid adducts to see if these are more suitable for a recovery process.

Separations Based Upon Water-Enhanced Solvation

We earlier found that solubilities of moderately soluble dicarboxylic acids in cyclic ketones are increased by factors of six to eight in the water-saturated solvent as opposed to the anhydrous solvent. Screening experiments and an examination of relevant data in the literature suggest that this phenomenon of enhanced solvation in the presence of water occurs for ketones, esters, nitriles and other hydrogen-acceptors as solvents, and for carboxylic acids and possibly for other hydrogen donors (such as phenols, alcohols, glycols and amides) as solutes. This phenomenon can be the basis for any of a variety of potentially energy-efficient separation processes, an example of which is regeneration of dicarboxylic acid extracts by selective evaporation of water, accompanied by precipitation of the dicarboxylic acid.

We are now screening candidate solute-solvent combinations to see which of these systems display sufficient water-enhanced solubility to be useful for separations of interest for this project. Initial experiments were attempted with high-performance liquid chromatography (HPLC) to determine the extent to which solute retention times are decreased in the presence of water in the carrier solvent. However, we could not locate a column which would give a sufficient delay of the peaks for solutes of interest without the column itself interacting chemically with the solute. We have now implemented vapor-headspace gas chromatography as a screening technique useful for studies of this effect with alcohols, monocarboxylic acids, and probably also glycols as solutes.

References

Chow TK, King CJ. *Separation of Compounds with Multiple -OH Groups from Dilute Aqueous Solutions via Complexation with Organoboronate*. Lawrence Berkeley Laboratory Report No. LBL-32430, May 1992.

King CJ. Recovering Carboxylic Acids by Extraction with Amine-Based Extractants and Sorbents. CHEMTECH, May 1992; 285-291.

King CJ, Starr, JN. Recovery of Carboxylic Acids by Precipitation from Organic Solutions. U.S. Patent No. 5,104,492. April 14, 1992.

King CJ, Tung LA. Sorption of Carboxylic Acid from Carboxylic Salt Solutions at pH's Close to or Above the pK_a of the Acid, with Regeneration with an Aqueous Solution of Ammonia or Low-Molecular-Weight Alkylamine. U.S. Patent No. 5,132,456. July 21, 1992.

Starr JN, King CJ. *Water-Enhanced Solubility of Carboxylic Acids in Organic Solvents and Its Application to Extraction Processes.* Lawrence Berkeley Laboratory Report No. LBL-31996, November 1991.

Starr JN, King CJ. Water-Enhanced Solubility of Carboxylic Acids in Organic Solvents and Its Application to Extraction Processes. *Ind. Eng. Chem. Res.* 1992; 31: 2572.

Tung LA, King CJ. *Recovery of Carboxylic Acids That Are Effective and Regenerable at $pH > pK_a1$* Preprints, Separations Division Topical Meeting, Miami Beach FL, Am. Inst. Chem. Engrs., 1992.

Investigators

C.J. King
R.R. Broekhuis
T.K. Chow
J.H. Lee
L.A. Tung

X-Ray Absorption Spectroscopy

Our goal is to develop new types of x-ray spectroscopy that will take advantage of the unique capabilities of the Advanced Light Source (ALS). Three new techniques are under development: x-ray magnetic circular dichroism, site-specific x-ray absorption, and flow-pump-probe spectroscopy. Experiments are conducted at the National Synchrotron Light Source (at Brookhaven) and the Stanford Synchrotron Radiation Laboratory (at SLAC).

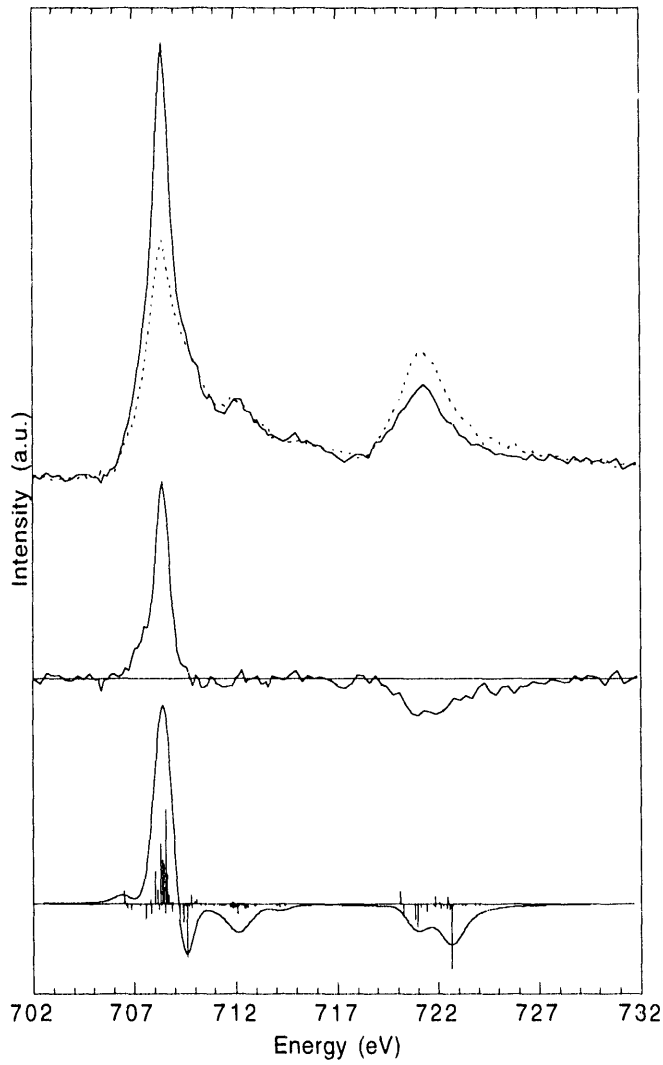

Figure 1.
XMCD spectrum of Fe in rubredoxin.

X-ray magnetic circular dichroism (XMCD) measures the difference in absorption of left- and right circularly polarized x rays by a sample in a magnetic field. This year we recorded the first x-ray magnetic circular dichroism spectrum of a paramagnetic sample, the Fe(III) center in the protein *rubredoxin* (Fig. 1). The effects are very large (about 40% absorption differences). The technique allows determination of the magnetic orientation of specific metal in different oxidation states, and should have broad application to bioinorganic chemistry and magnetic materials science.

Site-specific x-ray absorption is based on small shifts in fluorescence energies that occur with oxidation state changes. We have demonstrated fluorescence shifts (Fig. 2) for Mn(II), Mn(III), and Mn(IV), and are now building spectrographs to allow similar studies on Fe and Ni compounds.

The technique of flow-pump-probe spectroscopy has in the past been used with a laser pump and millimeter-scale hard x-ray probe beams. We are currently building an apparatus to use micron-sized soft x-ray probe beams from the Advanced Light Source, along with a pulsed dye laser pump beam. Upon completion, the smaller probe size will allow significantly shorter time scales to be examined.

References

Hubbard SR, Bishop WR, Kirschmeier P, George SJ, Cramer SP, Hendrickson WA. Identification and characterization of sites in protein Kinase C. *Science* 1991; 253: 1776.

Stojanoff V, Hamalainen K, Siddons DP, Hastings JB, Berman LE, Cramer SP, Smith G. A high-resolution x-ray fluorescence spectrometer for near-edge absorption studies. *Rev. Sci. Instrum.* 1992; 63: 1125.

Waldo GS, Mullins OC, Penner-Hahn JE, Cramer SP. Determination of the chemical environment of sulphur in petroleum asphaltenes by x-ray absorption spectroscopy. *Fuel* 1992; 71: 53.

George SJ, van Elp J, Chen J, Ma Y, Chen CT, Park J-B, Adams MWW, Searle BG, de Groot FMF, Fuggle JC, Cramer SP. L-edge x-ray absorption spectroscopy of *Pyrococcus furiosus* Rubredoxin. *J. Am. Chem. Soc.* 1992; 114: 4426.

Cramer SP, Chen J, George SJ, van Elp J, Moore J, Tench O, Colaresi J, Yocum M, Mullins OC, Chen CT. Soft x-ray spectroscopy of metalloproteins using fluorescence detection. *Nucl. Inst. Meth. A* 1992; 319: 285.

Mitra-Kitley S, Mullins OC, van Elp J, Cramer SP. Nitrogen chemistry in petroleum asphaltenes and coal by x-ray absorption spectroscopy. (*Fuel*, in press.)

Mitra-Kitley S, Mullins OC, Chen J, van Elp J, George SJ, Chen CT, O'Halloran T, Cramer SP. Nitrogen chemical structure in DNA and related molecules by x-ray absorption spectroscopy. *Biochem. Biophys. Acta* 1992; 1132: 249-254.

Mitra-Kitley S, Mullins OC, van Elp J, George SJ, Chen J, Cramer SP. Nitrogen in petroleum asphaltenes—local structure using fluorescence-detected soft x-ray absorption spectroscopy. (*J. Am. Chem. Soc.*, in press.)

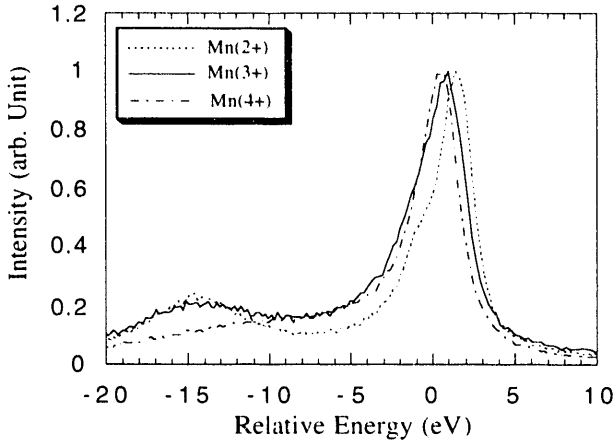

Figure 2.

Chemical shifts in manganese K fluorescence.

Hamalainen K, Kao C-C, Hastings JB, Siddons DP, Berman LE, Stojanoff V, Cramer SP. Spin-dependent x-ray absorption in MnO and MnF_2 (*Phys. Rev. B.*, in press.)

van Elp J, George SJ, Chen J, Peng G, Chen CT, Tjeng LH, Meigs G, Lin HJ, Zhou ZH, Adams MWW, Searle BG, Cramer SP. Soft x-ray magnetic circular dichroism—a new probe for studying paramagnetic bioinorganic systems. (Submitted to *Science*.)

Cramer SP, Chen J, Christiansen J, George SJ, Tittsworth R, Hales B, Coucouvanis D. EXAFS and L-edge spectroscopy of nitrogenase FeMo protein. Submitted to *Molybdenum Enzymes*, ACS Symposium Series (E. Stiefel, ed.).

George SJ, Lowery MD, Solomon E, Cramer SP. Copper L-edge spectral studies: A direct experimental probe of the ground state covalency in the blue copper site in Plastocyanin. (Submitted to *J. Am. Chem. Soc.*)

Chen J, George SJ, Tittsworth R, Hales BJ, Christiansen J, Coucouvanis D, Cramer SP. Iron EXAFS of *A. vinelanidii* nitrogenase Mo-Fe and V-Fe proteins. (Submitted to *J. Am. Chem. Soc.*)

Investigators

P. Cramer *X. Wang*
J. Chen *J. Moore*
J. van Elp

Ultrasensitive Laser Spectroscopies

DOE needs chemical sensors to detect and identify contaminants *in situ* at concentration levels not currently accessible using existing technologies. Some of the chemical contaminants include uranium, plutonium, lead, cadmium, chromium, trichloroethylene, benzene, carbon tetrachloride, and toluene. Small inexpensive optical fiber sensors are needed to address these chemical monitoring requirements. We have studied the development of optical fiber sensors using photothermal spectroscopies for monitoring actindes in aqueous samples. The photothermal techniques that have been developed include photoacoustic, photothermal deflection, and thermal lens spectroscopies. These spectroscopies provide measurements of optical absorption spectra at concentration levels approximately three orders of magnitude more sensitive than commercially available spectrometers.

Each of these photothermal techniques has been developed and tested in the laboratory using fiber optics to deliver the excitation light to the sample. A similar research effort exists at the Kernforschenzentrum, Institute for Radiochemistry (IRCH), Karlsruhe, Germany. This group has investigated the development of these photothermal techniques for measuring organic pesticides in aqueous environments. Through a collaborative International Technology Exchange Program, we compared/evaluated the photothermal techniques and other technologies for their suitability as remote sensors for environmental species.

We here summarize the research conducted by the LBL/LLNL and IRCH groups. Both the LBL/LLNL and IRCH groups emphasized development of a small, inexpensive optical fiber sensor based on thermal lens spectroscopy usingdiode lasers as excitation sources. Thermal lens spectroscopy (TLS) has been demonstrated in both laboratories to provide superior sensitivity compared to the other photothermal techniques, and TLS would not require electronic devices at the monitoring site. Only two fibers would be required—one to deliver the excitation light and a

second to monitor the optical absorption related to the chemical species. Such a sensor is envisioned to be only the size of a regular pen.

The IRCH also has initiated a research program in solid state microsensor technology. The areas of study include acoustic wave devices and chemical field effect transistors. IRCH is developing these technologies for detecting organic pesticides in aqueous environments at the ppm and ppb levels. A description of these microsensor technologies and their developmental status is presented.

Acoustic Wave Devices

Acoustic wave devices are frequency oscillators/detectors that offer ideal characteristics as chemical microsensors; they are small, rugged, and require only a nominal power supply. A typical surface acoustic wave (SAW) sensor device is approximately the size of a pen cap. These devices are commercially available in the MHz-GHz frequency regimes. An acoustic wave device is not a chemical sensor by itself, however; a chemical agent must be bound to the surface of the device to provide the selectivity and sensitivity to the chemical of interest. The raw device is composed of an interdigital transducer (IDT), lithographically deposited at each end of a small piece of piezoelectric crystal.

For the most common SAW device, a Rayleigh wave formed by exciting one IDT with a radio frequency voltage source travels across the device surface and is received by the second IDT. The Rayleigh wave energy, constrained to the surface, interacts strongly with any material in contact with the surface (*e.g.*, a chemically absorbent coating). Changes in the velocity of the acoustic wave are manifested as changes in the frequency of oscillation, similar to a quartz crystal microbalance. Precision is better than 1 part in 10 million.

SAW sensor research worldwide, including that at the IRCH, has focused primarily on detection of gas-phase organic and inorganic chemical species because SAWs are severely attenuated by the liquid and by the unavailability of suitable coatings. At the IRCH, other acoustic modes being evaluated include shear-horizontal and bulk (Lamb) waves. These modes have no displacements normal to the surface, or exhibit back-surface waves, respectively, and should be suitable for liquid-phase measurements. The devices are purchased at approximately $5 each and are used in the oscillator/delay line configuration. The primary effort has involved testing the stability and temperature characteristics of these devices when placed in aqueous environments without coatings. Because sensitivity to change increases as the square of the operating frequency, frequency is a parameter investigated in this work. A dual-channel acoustic-wave device is also being evaluated. Such a device could provide "on-sensor" frequency compensation for temperature, pressure, or other environmental factors. One channel of the device will be uncoated and the other channel coated with the chemical sensing agent. Currently, the research is limited by the unavailability of coatings suitable for liquid phase measurements.

Chem-FETs

Chem-FETs are microelectronics components, and like acoustic wave devices, they rely on a particular coating for chemical specificity. The technology is based on metal oxide semiconductor field effect transistor (MOSFET) circuitry. The MOSFET consists of two n-type diffusions, the source (S) and the drain (D) in a p-type silicon substrate. The structure is covered with an insulating layer of silicon dioxide on top of which a metal oxide gate electrode (G) is deposited over the area between source and drain. When a positive voltage is applied to the gate with respect to the source, electrons are attracted to the surface and create a conducting channel between source and drain. The conductivity of this channel can be modulated by the strength of the electric field that exists in the gate insulator between the metal gate and the silicon. Chemical sensing using MOSFET technology has been aimed primarily at ion detection, using the *ion-selective field effect transistor* (ISFET). For these sensors, the metal gate is removed and the insulator layer is exposed to an electrolyte solution containing the ion of interest. The ISFETs sensitivity to different ions can be made by depositing appropriate ion-selective membranes on the FET gate region. Chem-FETs are smaller and cheaper than ISFETs and require the deposition of a thin selective layer in the gate region. A chem-FET sensor can be as small as a pin head and cost less than $1. Applications of these devices as microsensors also are limited by the unavailability of coatings to make them sensitive and selective for the contaminant of interest.

References

Rojas D, Silva RJ, Russo RE. Thermal lens spectroscopy using a diode laser and optical fibers. *Rev. Sci. Instrum.* 1992; 63(5): 2989.

Shurig DA, Klunder GL, Shannon MA, Silva RJ, Russo RE. Signal analysis of transients in pulsed photoacoustic spectroscopy. (*Rev. Sci. Instrum.*, accepted for publication, February 1993)

[redacted] *Investigators* [redacted]

R.E. Russo
G.L. Klunder
J.D. Spear
R.J. Silva

*Nuclear Chemistry Division
Lawrence Livermore National Laboratory

Repetitively Pulsed Laser-Material Interaction and Steady-State Laser Sampling

The interaction of a high-energy pulsed laser beam with solid materials has a wide range of applications, including chemical analysis, thin-film fabrication, microfabrication, medical applications, and others. Laser-material interactions involve processes that range from heating of the target surface at low power density to the complicated violent ejection of materials (ablation) at high power density. The mode of energy coupling to the target depends on the laser wavelength, pulse duration, energy per pulse, and power density on the surface, as well as the properties of the target and the gas medium. It is desirable to minimize thermal processes, *e.g.*, heating, melting, and vaporization for many of these applications. For chemical analysis, the thermal component influences the stoichiometry of the sampled vapor through preferential vaporization. In addition, plasma formation and plasma shielding can reduce the laser energy coupled to the target, which reduces the efficiency of laser sampling and may lead to enhancement of thermal processes.

The explosive high-energy pulsed-laser material interaction (LMI) is not fundamentally understood. In our work, inductively coupled plasmaatomic emission spectroscopy (ICP-AES) was used for studying the behavior of the LMI. We demonstrated that the ICP is an excellent source for studying LMI because of its ability to dissociate refractory chemical species and excite the resultant atomized vapor to optical emission. We used ICP-AES to monitor the material vapor during laser sampling of copper by focusing a laser beam onto the sample surface at normal incidence with a 200-mm plano-convex lens. A 35 ps-Nd:YAG (266, 532, and 1064 nm) laser was used to study the effects of pulse duration on the interaction. The laser was pulsed at 10 Hz and 1500-3000 pulses were delivered to each location on the sample surface. A stream of carrier gas delivered the laser-sampled material to the ICP. The carrier gas is also the atmosphere in the laser sampling chamber. In this study, argon and helium gases were compared. After passing through the chamber, the carrier gas (Ar or He) merged with the other gas (He or Ar) with the same flow rate through a T-joint. The merged gas (Ar + He) then flows to the central channel of the ICP torch, the usual configuration for sample introduction. This procedure ensures that the gas composition in the ICP is constant, independent of the gas atmosphere in the chamber. ICP temperature and excitation characteristics will therefore be constant.

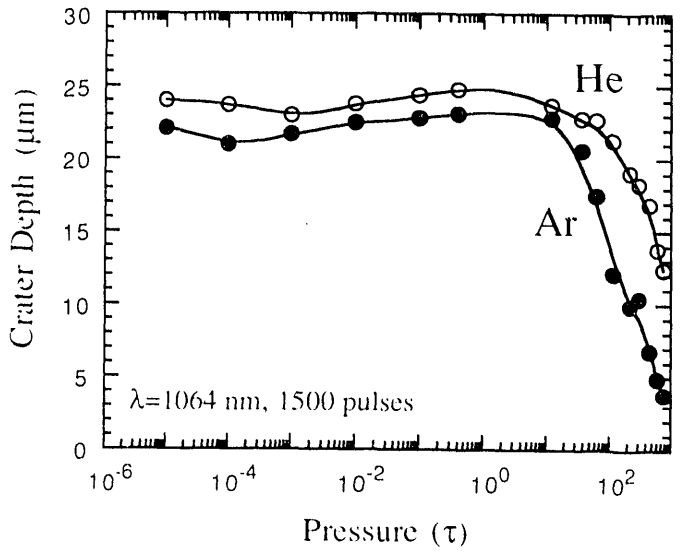

Figure 1.

Plot of crater depth for laser sampling of copper versus gas pressure for He and Ar gases. Open and closed circles are experimental crater depth data for He and Ar, respectively.

The thermal diffusivity of He is 26 times higher than that of Ar, and the ionization potential is 1.6 times higher. Ar is easier to ionize than He because of its higher ionization cross section, lower ionization potential, and slower heat dissipation. A plasma is more readily developed in Ar than in He. Therefore, plasma shielding is expected to be more severe in the Ar atmosphere, which is supported by our ICP-AES measurements. Using the fundamental frequency of the ps-laser, the He atmosphere improves the laser sampling rate of Cu. The Cu I 327.4-nm emission signal intensity in the ICP was 16 times higher using He (*vs.* Ar) in the sampling chamber. Examination of the crater shows corresponding behavior. In support of the enhanced ICP-AES data, the crater volume is greater in the He atmosphere for the same number of pulses. A larger crater in He atmosphere supports reduced plasma shielding mechanism and enhanced laser energy coupling to the sample, in agreement with the increased ICP-AES signal intensity.

The plasma shielding effect was further demonstrated by laser sampling Cu in He and Ar at different gas pressure. As the gas pressure is increased from 10^{-5} torr to 1 atm, a plasma forms more readily because of increased collisions; and plasma shielding is expected to be more significant at higher pressure. (A plot of crater depth for laser sampling of Cu *vs.* gas pressure for He and Ar gas is shown, Fig. 1). For both

He and Ar, crater depth is relatively independent of gas pressure lower than 10 torr. In Ar, crater depth begins to decrease significantly at pressures higher than 10 torr. A similar reduction is observed in He, except when starting at higher pressure of 100 torr.

We developed a model to describe this relation between the gas medium and a plasma based on inverse Bremsstrahlung absorption between the gas atoms and the fast electrons emitted from the target surface. During a picosecond laser pulse, the emitted atoms/ions only travel a few hundred Angstroms from the surface, assuming velocities on the order of 10^7 cm/s. The interaction (collisions) of the gas species with the ejected atoms and ions is negligible during the laser pulse, and the absorption of the laser photons (shielding) by the emitted atoms/ions to increase the ionized fraction in the plume can be ignored. However, a plasma (ionized plume) is initiated and plasma shielding does occur in this time regime due to the collisions of fast electrons (10^8 cm/s) with gas atoms. The model behavior was compared to measurements of the crater depth *vs.* gas pressure. At low pressure, both Ar and He are not ionized significantly by the inverse-Bremsstrahlung mechanism (Fig. 2; also plotted are the crater depth measurements of Fig. 1). Ionization occurs and increases drastically at about 20 and 150 torr for Ar and He, respectively. Although the data and model do not agree exactly with pressure, the behavior between the crater depth and the ionization of the gas medium are correlated. As the ionization increases, plasma shielding increases and the crater depth is reduced. The ionization rate is only approximate, as it does not account for other mechanisms of electron generation once the plasma is established.

The ICP-AES and crater volume data demonstrate that there is an effect of the gas medium on the laser ablation rate in the picosecond time domain. The depth of craters formed at different gas pressure was measured and the data correlate with our model describing gas ionization based on inverse-Bremsstrahlung absorption between fast photoelectrons and gas atoms. Plasma formation reduces the mass ablation rate and modifies the crater shape. Judicial selection of the gas medium and laser wavelength can improve the performance of the laser ablation for chemical analysis and other applications. The higher sampling rate in He than in Ar is beneficial to analytical applications. In turn, minimizing the plasma and laser-plasma interaction is likely to reduce the thermal component due to plasma radiation. By reducing the thermal component, preferential vaporization of high volatile elements in compound samples should also be minimized, thereby providing improved accuracy in chemical analysis.

References

Chan W-T, Mao XL, Russo RE. Differential vaporization during laser ablation/deposition of Bi-Sr-Ca-Cu-O superconducting materials. *Applied Spectroscopy* 1992; 46: 1025.

Chan W-T, Russo RE. Study of laser material interactions using inductively coupled plasma atomic emission spectroscopy. *Spectrochim. Acta* 1991; 46B: 1471.

Mao XL, Chan WT, Russo RE. Influence of gas medium on plasma shielding during laser material interactions in the picosecond time regime. (*Journal of Applied Physics*, submitted for publication)

Investigators

R. E. Russo
W.-T. Chan
X.L. Mao
M.A. Shannon
M. Kilgo

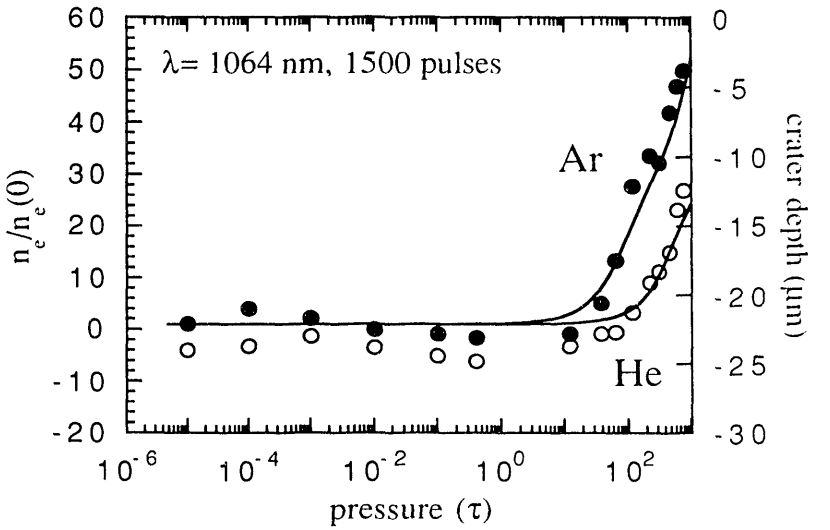

Figure 2.

Crater depth and electron density ratio versus gas pressure. Open and closed circles are experimental crater depth data for He and Ar, respectively. Solid curves correspond to the simulation of the change in ionization versus Ar and He gas pressure based on fast electron emission and inverse Bremsstrahlung, assuming initial electron temperature T_e = 10^5 K, electron density ne(0) =10^{17} cm^{-3}.

Bioorganometallic Chemistry: Bonding Studies of a (η^5-Pentamethylcyclopentadienyl)rhodium Aqua Complex to Nucleobases, Nucleosides, Nucleotides, and Sequence-Specific Oligonucleotides for Human Genome Applications

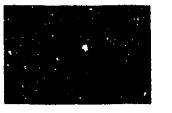

The Organometallic Chemistry group has focused on using an organorhodium aqua complex, $[Cp^*Rh(H_2O)_2(OTf)_2]_x$, to study its bonding modes with nucleobases, nucleosides, nucleotides, and sequence-specific oligonucleotides. These bonding studies were needed in order to develop a new technique to anchor single DNA molecules to the glass and electrode surface of an epifluorescence microscope for potentially mapping and sequencing the human genome.

New and innovative techniques are urgently needed in order to map and sequence the human genome; at present an extremely laborious and expensive undertaking.

We are pursuing a novel approach to this important problem, which utilizes organometallic-sequence-specific oligonucleotide complexes where a portion of the sequence-specific oligonucleotide of this organometallic complex recognizes complementary sequences in single DNA molecules and, as well, the organometallic metal center, bound to another portion of the sequence-specific oligonucleotide, acts as an anchor for the organometallic- sequence-specific oligonucleotide-DNA complex to the glass and electrode surface of the microelectrode stage of a epifluorescence microscope. The anchored single DNA molecule is visualized with ethidium bromide as the fluorescence label, and then selectively cut by optical methods, and manipulated on the microelectrode stage of the epi-fluorescence microscope; a technique, along with Polymerase Chain Reaction (PCR) amplification, for physical mapping and sequencing single DNA molecules.

In order to develop this novel technique, it will be necessary to extensively study the binding of the water-soluble organometallic complexes to nucleobases, nucleosides, nucleotides, sequence-specific oligonucleotides, and to model glass silica surfaces. We propose to use a water-soluble (η^5-pentamethylcyclopentadienyl)rhodium aqua complex for these purposes with structural analyses of the metal-DNA base complexes by high-field nuclear magnetic resonance spectroscopy (NMR), circular dichroism (CD), FAB mass spectrometry (FAB-MS), Uv-Vis spectroscopy (Uv-vis), infrared spectroscopy (IR), molecular graphic techniques, graphite furnace atomic absorption spectroscopy (GFAA) and also characterized, when possible, by single-crystal x-ray analysis.

Reference

Smith DP, Baralt E, Morales B, Olmstead MM, Maestre MF, Fish RH. Bioorganometallic chemistry, 1. Synthetic and Structural Studies in the Reactions of a Nucleobase and Several Nucleosides with a (η^5-pentamethylcyclopentadienyl)-rhodium Aqua Complex. *J. Am. Chem. Soc.* 1992; 114: 10697.

Investigators

R.H Fish
D.P. Smith
M.F. Maestre
M.M. Olmstead

Material Applications

High-Temperature Superconducting Thin Films for Tape Conductors

The idea for this project was that the high critical current densities readily achieved with high-temperature superconducting epitaxial films on single crystals may also be possible on practical metal substrates, if suitable, highly specialized, buffer layers can be developed. This concept was risky due to the intractable nature of the weak link problem in $YBa_2Cu_3O_7$. That is, "weak links" impede current flow across high-angle grain boundaries. Nonetheless, high critical current densities have been achieved, as reported here.

A sufficient condition for successful $YBa_2Cu_3O_7$ (YBCO) film growth is the growth of a suitable buffer layer, since high-current films are readily formed on single-crystal substrates. During 1990 and 1991, our efforts focused on buffer layer morphology and orientation. The material yttria stabilized zirconia (YSZ) worked particularly well as a buffer layer. Conditions for laser deposition of this material with controlled (001) orientation normal to the substrate were achieved by careful adjustment of oxygen pressure and substrate temperature. The overlying YBCO films reached a plateau of quality, however, because the YBCO grains, like the YSZ crystallites, were randomly oriented in the plane of the film.

To develop methods for in-plane alignment of the buffer layer, we considered a number of techniques, including grapho-epitaxy (epitaxy using a lithographic pattern) and oblique angle deposition. However, the most promising method so far has proved to be ion-assisted deposition. While the buffer layer is formed by the laser ablation process, it is bombarded by inert Ar ions from an oblique angle. The proposed mechanism is that crystallites which nucleate with the wrong orientation are sputtered away by the ion beam, while crystallites which form with an ion channeling orientation can grow. A group in Japan [Iijima et al., *Appl. Phys. Lett.* 60, 769 (1992)], working independently of LBL, also managed to achieve the necessary in-plane orientation in the buffer layer. In their case the

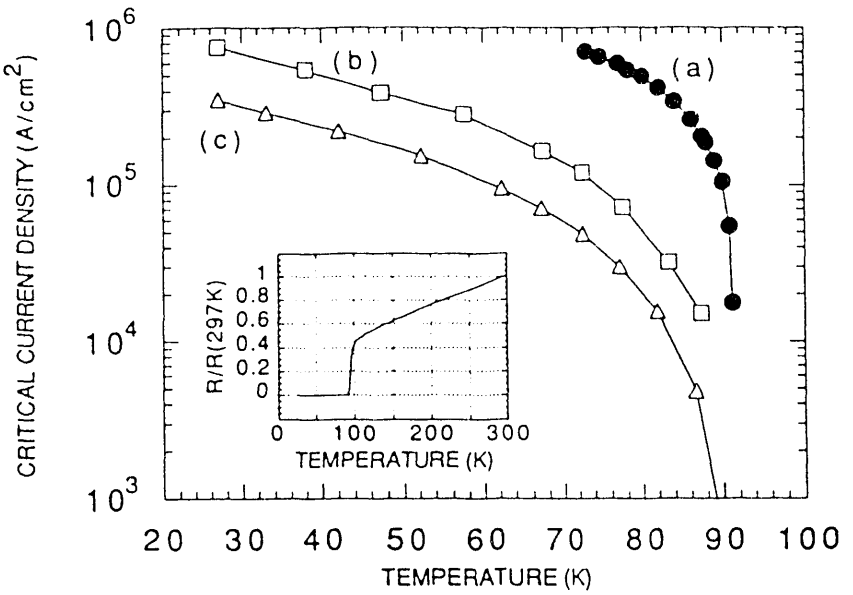

Figure.

Critical current density for YBCO thin film on buffered metal substrate (a) without magnetic field; (b) with 0.4 tesla field parallel to the film; and (c) 45° to the film normal, the direction for which the current capacity is lowest. Inset shows normalized resistance vs. temperature.

buffer layer is grown by sputtering rather than laser ablation. This is the only other group currently reporting very high critical currents in YBCO films on metal substrates.

Our best film on metal substrate (YBCO on YSZ buffer layer) had T_c of 92 K, J_c(77K, 0T) = 6 × 105 A cm^{-2}, J_c(77K, 0.4 T) = 8 × 104 A cm^{-2}. The figure (below) shows how the critical current density increases further as the temperature is lowered. The original program goals of 104 A cm^{-2} at 35 K and 2 T have been exceeded by about a factor of 30. (The first reference gives detailed data on this film.)

These new films mark an important milestone in the development of high-temperature superconducting tapes for application as high-power electrical conductors and for the fabrication of magnets, motors, and generators, for example.

References

Reade RP, Berdahl P, Russo RE, Garrison SM. Laser deposition of biaxially-textured yttria-stabilized zirconia buffer layers on polycrystalline metallic alloys for high critical current Y-Ba-Cu-O thin films. *Appl. Phys. Lett.* (in press, 1992).

Berdahl, P, Mao XL, Russo RE, and Yin E. Angular magnetoresistance provides texture information on high-Tc conductors. *Physica C* 1992; 195:93.

Yin E, Rubin M, and Dixon M, Sputtered YBCO films on metal substrates. *J. Mater. Res.* 1992; 7:1636.

Faulques E, and Russo RE, Raman spectra of iodide species in intercalated $IBi_2Sr_2CaCu_2O_8$. *Solid State Commun.* 1992; 82:531.

Lam QH, Jeffries CD, Berdahl P, Russo RE, and Reade RP. Complex ac permeability and harmonic generation of a thin film of $YBa_2Cu_3O_{7-x}$: measurements and models. *Phys. Rev.* 1992; 46:437.

Berdahl P, Reade RP, Rubin M, Russo RE, and Yin E. Angular magnetoresistance of textured thin-film conductors. In: R. Singh, M. Nisenoff, and D. Pavuna, eds. Progress in High-Temperature Superconducting Transistors and Other Devices II. *Proceedings of the SPIE*, 1992; 1597:64.

Investigators

P. Berdahl
R. Reade
R. Russo

Microstructured Materials: Light-Scattering Properties of Marine Microorganisms

The goal of this research is to investigate and predict the optical properties of ocean water by modeling and measurement of the light scattering from ensembles of spherical and nonspherical marine micro-organisms and to evaluate the effects of that scattering on visibility, irradiance, and transmission of polarized and unpolarized light in the ocean. As part of this goal, we are studying the interaction of polarized light with optically-active unicellular marine organisms with chiral and non-chiral structure in order to clarify the causes and effects of polarized light in the ocean.

To study light scattering from chiral organisms, the helical sperm head of the octopus, *Eledone cirrhosa*, was chosen as a model system for measurement and modeling of polarized-light scattering from non-spherical particles. It is an excellent system because it is well-characterized and, being helical, it produces strong effects on the polarization state of scattered light. To characterize the light scattering from this system of particles, the angular dependence of all 16 elements of the Mueller Scattering Matrix (S_{ij}) were measured for the first time. The 16 elements of this matrix completely characterize the inelastic scattering from any system. The angular dependence of one matrix element, S_{14}, (indicative of circular polarization effects) agreed with earlier measurements. The wavelength dependence of this element was consistent with the idea that S_{14} increases as the pitch of the helix approaches the wavelength.

Different approaches to calculating the polarized light scattering from the octopus sperm were explored. A model based on the first Born approximation of a continuous helix was developed and compared to models using discrete dipoles to represent the helix. Two models using discrete dipoles were explored. A model based on noninteracting dipoles (independent-dipole model) is essentially the first Born approximation, but for discrete scattering centers. The second model included the interaction between the dipoles and is referred to as the coupled-dipole model. The Born approximation was used to predict all 16 elements of the Mueller matrix for a single continuous helix at any orientation with respect to the incident light and to obtain an analytical average for the Mueller matrix for an ensemble of randomly-oriented helices made of point polarizable groups.

Predictions from the continuous-Born and independent-dipole models differ if an insufficient number of discrete subunits used to represent the helix. These differences can be used to determine the number of dipoles needed to describe a given helix. For helices whose radius or pitch is large compared to the wavelength of light, many dipoles are needed to accurately calculate the Mueller matrix elements. A supercomputer is limited to calculating scattering from a helix of 1200 dipoles when interactions are included. Therefore, when the pitch and radius of the helix are larger than the wavelength of light and the thickness of the body of the helix is accurately modeled by the polarizability input, the continuous-Born model may yield the best results. In general, the continuous-Born model is the least computer intensive of the three models.

The importance of including interactions between dipoles in scattering cal-

culations for a single stranded-helix depends on the relative dielectric constant of the helix, its thickness, and the degree of anisotropy of the individual dipoles (represented by the aspect ratio of the subunit used to model the helix). For a thin helix, the applicability of the independent model can be extended by using larger aspect ratios for materials with higher dielectric constants. Thus, the need for a high aspect ratio limits independent-dipole modeling to thinner helices to guarantee that the dimensions of the subunits of the helix be sufficiently small relative to the wavelength of light. For small relative dielectric constants, the aspect ratio can be 2:1 without the need to include dipole interactions, thus one can adequately model a helix with a strand thickness of 1/10 the wavelength of light without having to include interactions. A helix with strand thickness of the order of the wavelength of the light must be modeled with several strands. The number of subunits needed per strand to accurately describe the helix probably does not decrease as more strands are introduced. Therefore the application of the coupled-dipole approximation to thicker helices requires considerable computational capability. The Born approximation was also used to calculate the orientational average of many helices to predict the behavior of a solution of helical particles. It was found that the calculated averaged value of the S_{34} Mueller matrix elements was zero. However, this result is inconsistent with measurements of the octopus sperm heads, and therefore indicates that the Born approximation cannot be used to predict this matrix element.

Measurements of the Mueller matrix of helical particles (octopus sperm heads) were compared to theoretical approaches in order to establish practical models of polarized light scattering from helical or other non-spherical particles. Guidelines for the number of polarizable groups needed to describe a helix and the importance of including interactions between these groups were established for coupled dipole theory in modeling single stranded helices. This work established a basis for calculating scattering from a variety of different shaped structures by developing a methodology for representing and calculating scattering from an array of points or continuous linear shapes.

Reference

Lofftus KD, Quinby-Hunt MS, Hunt AJ, Livolant F, Maestre M. Light scattering by *Prorocentrum micans*: a new method and results. *Applied Optics* 1992; 231: 2924.

Investigators

A. Hunt
K. Kuah
P. Hull
M. Quinby-Hunt
D. Shapiro

Microstructured Materials: Development of Improved Aerogel Superinsulation

This research is being carried out to develop methods to produce new microporous materials based on sol-gel processing and supercritical solvent extraction. Currently, the primary direction of the research is to improve the thermal insulating properties of silica aerogel by adding additional phases to form aerogel composites. This year we have extended this research into the more general area of nanostructured materials based on aerogel composites.

We are also continuing various technology transfer efforts to encourage the commercialization of aerogel-based materials. The thermal resistance of aerogel has been substantially improved by adding another component to the aerogel. New superinsulating materials based on this approach can replace existing CFC-containing polyurethane insulation and at the same time significantly improve the thermal efficiency of refrigerators and freezers, reduce heat losses in hot and cold piping, insulate batteries in electric vehicles, and reduce energy losses in a variety of other applications. The improvement of thermal performance has two main benefits: it lowers the cost of the aerogel by as much as 30%, making it more competitive with other advanced insulations, and it provides the same thermal performance in thiner layers for space sensitive-applications.

We are preparing and characterizing the new aerogel composites and studying analytically the effect of dopant materials on heat transfer within the aerogel. The thermal resistance of aerogel can be substantially increased by adding infrared absorbing compounds or introducing structural modifications to inhibit the radiative heat transfer by scattering. In evacuated silica aerogel at ambient temperatures, this radiative component is responsible for up to half or more of the thermal conductivity; therefore its reduction will substantially improve the thermal performance of aerogel insulation. At elevated temperatures (200° to 500°), the radiative component of heat transfer in aerogel becomes dominant. The effective suppression of the infrared radiation by the methods under development can provide insulating materials with vastly improved thermal performance for a number of industrial applications.

The thermal resistance of undoped silica aerogel (R-20/inch at ambient temperature for evacuated aerogel) can be substantially improved by blocking the thermal radiant transfer in 3-8 and 12-16 micron regions in the infrared. This is because silica has low intrinsic absorption in the 3-8 micron region and the radiation can be blocked by adding a finely dispersed absorber. In the longer-wavelength region, dense structural additives can produce scattering. We have been investigating methods to add inexpensive absorbing materials to aerogel that absorb infrared radiation, are compatible with the sol-gel and supercritical drying process, are stable to higher temperatures, and improve aerogel's compressive strength.

Alcogel samples were prepared and supercritically dried using the carbon dioxide substitution developed at LBL.

Infrared transmission measurements are made directly on the thin aerogel samples or by preparing powders for dispersion in pressed KBr pellets. Carbon was found to be the best additive for blocking the infrared transmission. After developing methods to prepare improved materials, larger gels were poured and dried under an arrangement with Thermalux L.P. (Richmond, CA). Samples twelve inches in diameter were produced and thermal measurements performed by an independent contractor. The highest thermal resistance reached so far was R-32 per inch (more than a 50% performance increase over undoped aerogel). Further improvement is expected if higher strength aerogel can be developed. This would enable lower density materials and thereby lower the solid component of thermal conductivity.

To analyze and predict the thermal performance of opacified aerogel the infrared heat transfer inside aerogel was modeled. The objective is to predict the thermal conductivity as a function of temperature using the infrared absorption measurements. A thermal diffusion model was used with the absorption data to calculate the wavelength-dependent spectral-flux within the aerogel. Spectral flux plots were used to determine the wavelength regions responsible for contribution to the thermal conductivity at various temperatures and integrated to obtain the thermal conductivity as a function of temperature. The predicted effects of carbon doping on the thermal performance of aerogel are quite dramatic at temperatures from 200 to 500°C and if borne out, opacified aerogel will be an outstanding medium temperature insulating material.

We have been exploring the preparation of a whole new family of nanoporous composite materials based on the methods we developed to opacify aerogels. In addition to achieving high densities of carbon in the silica aerogel, nanophase composites were prepared using elemental silicon and iron. Aerogel composites of the oxides of iron, nickel, and copper were also synthesized. Use of these methods appears to allow production of a wide variety of new composites. Such nanophase materials have potential applications in magnetic cooling cycles, electroluminescent displays, and for transparent magnetic materials.

Technology-transfer activities undertaken during the year included visits to industries (aerospace, automobile, insulation, and others) to acquaint the technical and managerial staff with the properties of aerogel and to identify new applications specific to that industry.

References

Hunt AJ. Optical and thermal properties of silica aerogels. In: L.H. Hench and J.K. West, eds. *Chemical Processing of Advanced Materials*. New York: John Wiley & Sons, 1992.

Hunt AJ. Aerogel--A Transparent, Porous Superinsulator. In: *Proceedings of the ASCE*, Atlanta, GA, August 10-12, 1992.

Investigators

A. Hunt
W. Cao
E. Chen
N. Fetter
S. Zeng

Projects described in this report were supported by the following sources:

- U.S. Department of Energy, Assistant Secretary for Conservation and Renewable Energy:
  - Office of Energy Management, Office of Utility Technologies, Advanced Utility Concepts Division
  - Office of Transportation Technologies, Electric and Hybrid Propulsion Division
  - Office of Industrial Technologies, Advanced Industrial Concepts Division, Advanced Industrial Materials (AIM) Program
  - Office of Utility Technologies, Advanced Utility Concepts Division
- U.S. Department of Energy, Office of Energy Research, Office of Basic Energy Sciences, Chemical Sciences Division
- Morgantown Energy Technology Center, Assistant Secretary for Fossil Energy, Office of Coal Utilization, Advanced Research and Technology Development, Division of Surface of Coal Gasification
- Lawrence Livermore National Laboratory Contract No. W-7405-ENG-48
- Electric Power Researh Institute (EPRI)
- Laboratory-Directed Research & Development Funds
- Office of Naval Research, Environmental Scinces Program

This support was provided through the U.S. Department of Energy under Contract No. DE-AC03-76SF00098

DATE
FILMED
9/29/93

END